Aalborg Universitet

Small-Signal Modeling of AC Power Electronic Systems: Critical Review and Unified Modeling

Liao, Yicheng; Wang, Xiongfei

Link to publication from Aalborg University

Small-Signal Modeling of AC Power Electronic Systems: Critical Review and Unified Modeling

YICHENG LIAO [1] (Member, IEEE), AND XIONGFEI WANG [2] (Senior Member, IEEE)

[1] School of Electrical Engineering and Computer Science, KTH Royal Institute of Technology, SE-100 44 Stockholm, Sweden
[2] AAU Energy, Aalborg University, 9220 Aalborg, Denmark

CORRESPONDING AUTHOR: XIONGFEI WANG (e-mail: xwa@energy.aau.dk)

ABSTRACT The harmonic state-space (HSS), the dynamic phasor (DP), and the generalized dq (GDQ) modeling are three widely used methods for small-signal analysis of ac power electronic systems. By reviewing their principles and deriving their mathematical relationships, this paper proposes a unified framework for all the three approaches. The unified modeling reveals that the linearization and transformation can be exchanged flexibly in the modeling process, and the initial phase takes a role in transforming the GDQ model into the HSS or DP model. Case studies on a three-phase voltage-source converter in unbalanced power grids are provided for validation. The relationships of three modeling methods are verified by mathematical proofs and time-domain simulations. The unified frequency-domain model is further validated through the frequency scan in experiments. Insights of the unified modeling framework and recommendations from engineering perspectives are finally discussed.

INDEX TERMS AC power electronic system, dynamic phasor modeling, generalized dq modeling, harmonic state space modeling, small-signal modeling, time-periodic systems.

I. INTRODUCTION

AC power electronic systems are widely found in modern power grids, driven by the large-scale integration of renewable energy resources, flexible dc and/or ac transmission systems. The dynamic interactions of these ac power electronic systems may lead to resonances and abnormal harmonics across a wide frequency range [1]. It is of paramount importance to model and analyze the dynamics of converter-based power systems. The linearized modeling methods are commonly used, as they allow the use of small-signal dynamic analysis tools, e.g. the eigenvalue- or the impedance-based methods.

To retain control dynamics of ac converter-based systems, the state-space averaging (SSA) over the switching period is generally applied [2], [3], which yields an averaged dynamic model that is essentially nonlinear and time-periodic. The conventional way to model such systems is to apply first the Park transformation to establish a time-invariant system in the synchronous reference (*dq*) frame, and then perform the linearization around equilibrium points of the system to obtain a linear time-invariant (LTI) model [4]. The *dq*-frame model can be represented with real vectors [5], [6] or complex vectors [7]–[10], and even be transformed back to the stationary

reference (*αβ*) frame [11], [12]. However, these LTI models are only valid in three-phase balanced power systems. In the presence of three-phase unbalanced or even harmonically distorted voltages, the time periodicity is still present in the *dq* frame, and their dynamics cannot be characterized as the LTI model in the single *dq* frame.

To characterize the time-periodic dynamics in unbalanced or harmonically distorted ac systems, three modeling methods have been developed: 1) the harmonic state space (HSS) modeling [13]–[18]; 2) the dynamic phasor (DP) modeling [19]–[22]; 3) the generalized *dq* (GDQ) modeling [23]–[25].

The HSS modeling method characterizes the frequency-domain dynamics of linear time-periodic (LTP) systems [26], thus a prior linearization around the steady-state trajectories is required [27], [28]. The HSS model results in a harmonic transfer function (HTF) in the frequency domain, which is, essentially, an LTI transfer function matrix, revealing dynamic couplings between the Fourier coefficients of harmonics [29]. The HSS modeling has been used for dynamic analyses of single-phase converters [13], modular multilevel converters [15], [16], and three-phase converters in unbalanced grids [17], [18]. While originally derived with the real-valued LTP

models, it is later found that the HSS model can also be used to represent complex-valued LTP models, which facilitates the integration of closed-loop control dynamics into power stages of converters [16], [17], [30].

The DP modeling is derived from the generalized averaging (GA) operator [31], [32]. Given a fixed system fundamental frequency, the GA operator calculates the Fourier coefficients of time-periodic variables over a moving time window [31], thus the time-periodic system can be represented by the differential equations of multiple time-invariant Fourier coefficients. Then, the linearization around their equilibrium points can be performed [33]. This method has been widely applied to model power converters in three-phase unbalanced grids [19], [22] or with multiple harmonics [20], [21]. The GA operator can be applied in any reference frame wherever the system is time periodic, and it can be represented with either real-valued or complex-valued variables [22].

The GDQ modeling method is developed based on the GDQ transformation theory [23]. The GDQ transformation allows for modeling the time-periodic system in multiple *dq* frames, where only the dynamics around the time-invariant operating points need to be considered, which can be achieved by further applying an SSA operator. The idea was initiated in [34] to model an unbalanced ac system. However, the multiple *dq*-frame model in [34] overlooked the couplings between different *dq* frames, due to the time-periodic nature of the resulted systems in each *dq* frame. This flaw was addressed in [23] by invoking the principle of harmonic balance [35]. The GDQ modeling has recently been applied to multi-level modular converters [24], [25].

The three modeling methods have been developed based on different principles for a long time, until a few recent works exploring their relationships. The equivalence between the HSS model and DP model has been implicitly discussed in [36], by showing that the DP model yields the same state-space matrices as the HSS model. Their relationships were further more thoroughly studied in [33], [37]–[41]. In [37], the DP model was claimed as less accurate than the HSS model, considering that the high-frequency dynamics was assumed to be neglected for the DP model, which was imprecise due to the improper assumption. In [33], the different linearization principles of the two methods were emphasized, i.e., the HSS model is based on linearization around the time-periodic trajectories, whereas the DP model is based on linearization around the time-invariant points. In [38], the equivalence of the two methods was verified through the eigenvalue analysis of the resulted state-space models, which was, however, merely based on numerical studies. Their relationship is further revealed in [39], pointing out that the DP model can be transformed into the HSS model through the Laplace transformation. The equivalence between the GDQ model and the DP model was reported in [40] with the proofs in the complex space. The equivalence of the GDQ model and HSS model was also studied in [41] based on the principle of harmonic balance. However, these works assume that the initial phase used for the GDQ transformation is zero, which is valid when

studying a single converter system, where the initial phase reference of the converter terminal voltage can be assumed as zero. However, when there are multiple converters connected with line impedances, the initial phases of different converter voltages are dependent on the power flow, and each converter needs to be linearized around its terminal voltage, where the initial phases of voltages cannot be assumed as zero [8], [12], [42].

Whereas the above attempts have discussed the relationships of these modeling methods, how to interpret these methods in modeling ac systems has not been clearly contemplated. The major challenges lie in the following aspects:

- Refs. [33] and [39] only discuss the modeling of frequency couplings caused by switching dynamics in dc converter systems. In addition to the switching dynamics, the most important nonlinearity in ac converter systems originates from the trigonometric functions, which are involved in the ac-dc modulation of the converter power stage and the Park or inverse Park transformation used in the converter control. These trigonometric functions can introduce different frequency coupling dynamics compared with dc converter systems. However, how to interpret the mathematical relationships of different modeling methods on the linearization of trigonometric functions still remains unclear.
- Refs. [33], [38] and [39] mainly distinguish the HSS modeling and DP modeling from the modeling procedures. However, the relationships between the linearization and transformation have not been fully understood for these modeling methods.
- The impacts of the initial phases for the GDQ modeling of ac systems are not considered in the existing studies [40], [41]. The existing studies on the initial-phase effect [8], [42] are merely for modeling balanced ac systems in a single *dq* frame. Its impact on modeling an unbalanced ac system in multiple *dq* frames has not been discussed.

This work is thus dedicated to address these challenges, by developing a unified modeling framework for ac converter-based systems. Some missing mathematical relationships among the three modeling methods are revealed. The unified modeling framework is further verified on a three-phase converter under unbalanced grids through mathematical proofs, simulations, and experiments.

II. FUNDAMENTALS OF LINEARIZED MODELING
The fundamentals of the HSS modeling, DP modeling and GDQ modeling are revisited in this section, which in general cover three steps: 1) the equilibria representation, 2) the small-signal linearization, and 3) the frequency-domain modeling.

In the following derivations, it is assumed that the converter switching dynamics are neglected through an averaging operator over the switching period, since this work focuses on the linearization of trigonometric functions in ac systems. Moreover, the converter modeling is discussed in more generic grid conditions, where multiple harmonics can be present in steady states. Variables without any subscript, e.g., $x(t)$, can be

defined in any reference frame and can be either real-valued or complex-valued. If with the subscript "$\alpha\beta z$" or "dqz", the variables are defined in that reference frame. Variables in bold letters, e.g., $\mathbf{x}(t)$, indicate the complex-valued variable representation. The $\alpha\beta$-frame complex variables are defined as $\mathbf{x}_{\alpha\beta} = x_\alpha + jx_\beta$ and $\mathbf{x}_{\alpha\beta}^* = x_\alpha + jx_\beta$, and similar definitions apply to dq-frame complex variables. Variables with capital letters or the subscript "0" represent the equilibrium point or the steady-state trajectory, respectively. "Δ" before variables denotes the small-signal dynamics. $\mathbb{Z}$ denotes the integer set, $\mathbb{R}$ denotes the real number set, and $\mathbb{C}$; denotes the complex number set.

A. EQUILIBRIA REPRESENTATION

The equilibria representation is the prerequisite for the linearized modeling. The HSS modeling starts with the time-periodic representation of system equilibria. In normal operations, any variable in an ac system, denoted by x, travels along a trajectory or orbit periodically [43]. Thus, this trajectory can be represented by a time-varying variable $x_0(t)$, which satisfies

$$x_0(t) = x_0(t + T) \in \mathbb{R} \text{ or } \mathbb{C}. \tag{1}$$

where T is the fundamental period of the time (T)-periodic system. In a generic ac system, multiple frequency components of $k \cdot f_s$ may be present under grid unbalance or harmonic distortion, thus, $f_s = 1/T$ ($\omega_s = 2\pi/T$) can be chosen as the largest common factor of the existing frequency components.

Alternatively, a time-periodic trajectory can be equivalently represented by a set of time-invariant operating points through some transformations. The principle is to use transformations to map the ac system from the original space into a new space with an orthogonal basis. In the new space, all the coefficients of the orthogonal basis are time-invariant and independent to each other, thus, further linearization can yield a LTI model, which allows using the classical LTI analysis tools for dynamic studies. The DP modeling and GDQ modeling are based on this principle.

For DP modeling, it is assumed that the system steady-state trajectory can be presented based on Fourier series expansion, i.e.,

$$x_0(t) = \sum_k X_k e^{jk\omega_s t} \in \mathbb{R} \text{ or } \mathbb{C} \tag{2}$$

Thus, the equilibria of a T-periodic system can be represented by the time-invariant Fourier coefficients, i.e., $[\cdots X_{-k} \cdots X_k \cdots]^T$, with the set of exponential functions $\{k \in \mathbb{Z}|e^{jk\omega_s t}\}$ serving as an orthogonal basis [44]. The generalized averaging (GA) operator can be used to calculate the Fourier coefficients [31], i.e.,

$$\langle X \rangle_k = \frac{1}{T} \int_{t-T}^{t} x_0(\tau) e^{-jk\omega_s \tau} d\tau = X_k \text{ for } k \in \mathbb{Z}, \tag{3}$$

For the GDQ modeling, it applies the generalized dq (GDQ) transformation [23] to ac variables obtain time-invariant
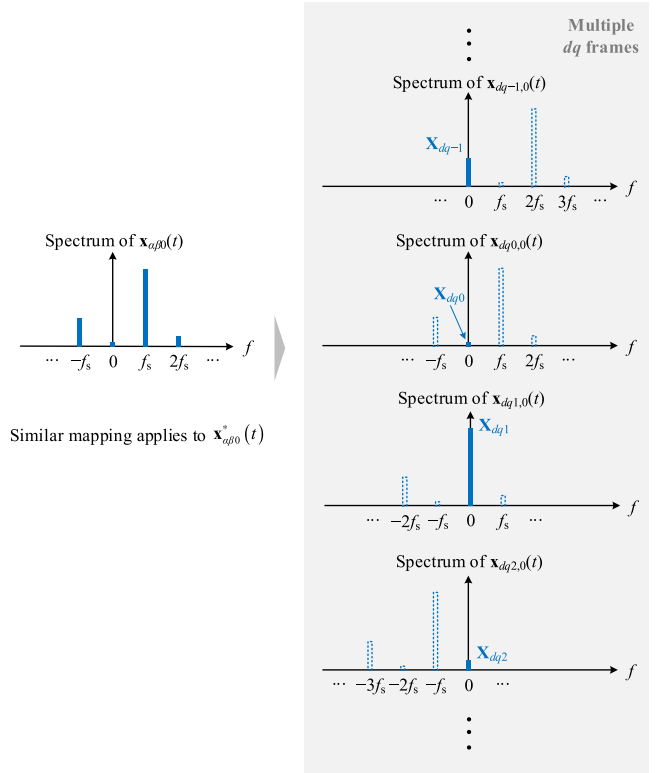

FIGURE 1. Illustration of time-invariant representations in multiple *dq* frames for the GDQ modeling.

representations in multiple dq frames, which is given by

$$\begin{bmatrix} x_{dk,0} \\ x_{qk,0} \\ \vdots \\ x_{d-k,0} \\ x_{q-k,0} \end{bmatrix} = \begin{bmatrix} \cos\theta_k & \sin\theta_k & & \\ -\sin\theta_k & \cos\theta_k & & \\ & & \ddots & \\ & & \cos\theta_{-k} & \sin\theta_{-k} \\ & & -\sin\theta_{-k} & \cos\theta_{-k} \end{bmatrix} \\ \times \begin{bmatrix} x_{\alpha 0} \\ x_{\beta 0} \end{bmatrix}, \tag{4}$$

where $\theta_k = k\omega_s t + \varphi_k$ and $\theta_{-k} = -k\omega_s t + \varphi_{-k}$ are the phases of the positive and negative k-th harmonic components, and their initial phases can be different. The GDQ transformation can be also represented with complex variables [7] as

$$\begin{bmatrix} \mathbf{x}_{dqk,0} \\ \mathbf{x}_{dqk,0}^* \\ \vdots \\ \mathbf{x}_{dq-k,0} \\ \mathbf{x}_{dq-k,0}^* \end{bmatrix} = \begin{bmatrix} e^{-j\theta_k} & 0 \\ 0 & e^{j\theta_k} \\ \vdots & \vdots \\ e^{-j\theta_{-k}} & 0 \\ 0 & e^{j\theta_{-k}} \end{bmatrix} \begin{bmatrix} \mathbf{x}_{\alpha\beta 0} \\ \mathbf{x}_{\alpha\beta 0}^* \end{bmatrix}. \tag{5}$$

However, the exponential operators in (5) indicate that the GDQ transformation itself only results in frequency shifts of the original ac variable by the phase rotations. Fig. 1 shows a graphical illustration for the GDQ transformation. Taking $\mathbf{x}_{\alpha\beta 0}(t)$ as an example, if it has multiple harmonics, the resulted dq-frame variables $\mathbf{x}_{dqk,0}(t)$ are also time-periodic,

whose spectra are merely shifted from the spectrum of $\mathbf{x}_{\alpha\beta 0}(t)$. It can be found that using all the dc components in $\mathbf{x}_{dqk,0}(t)$, i.e., $\mathbf{X}_{dqk}$ denoted by the solid bars, is sufficient to represent the original spectrum of $\mathbf{x}_{\alpha\beta 0}(t)$. The harmonic components in $\mathbf{x}_{dqk,0}(t)$, as denoted by the dashed bars, are redundant. That is to say, to obtain the time-invariant representations in multiple dq frames, it is required to further apply an SSA operator, i.e.,

$$\left[\mathbf{x}_{dqk,0}, \mathbf{x}_{dqk,0}^*\right]^{\mathrm{T}} \overset{\text{SSA}}{\to} \left[\mathbf{X}_{dqk}, \mathbf{X}_{dqk}^*\right]^{\mathrm{T}}, \tag{6}$$

where the averaging time window is chosen as the fundamental period of the resulted dq-frame variables. By applying the averaging operator, the reversibility of the GDQ transformation can be ensured. The original ac variable can thus be represented as

$$\begin{bmatrix} \mathbf{x}_{\alpha\beta 0} \\ \mathbf{x}_{\alpha\beta 0}^* \end{bmatrix} = \sum_k \begin{bmatrix} e^{j\theta_k} & 0 \\ 0 & e^{-j\theta_k} \end{bmatrix} \begin{bmatrix} \mathbf{X}_{dqk} \\ \mathbf{X}_{dqk}^* \end{bmatrix}. \tag{7}$$

It can be seen that the GDQ transformation with averaging also realizes a linear representation of the original ac variables with time-invariant dq-frame variables, where the orthogonal basis is the set of exponential function matrices for all k shown in (7). This builds the basis for the GDQ modeling.

It is worth noting that the GDQ transformation and averaging only realize the time-invariant representations of ac variables. In a converter system, there are always interactions between the ac and dc variables, the latter of which can be dc-side voltage, dc-side current, active and reactive powers, etc. It is also necessary to find time-invariant representations of dc variables at the same time, which can be obtained through the GA operators.

With such time-invariant representations of the system equilibria, the dynamics of the original system can be equivalently modeled by higher-order differential equations of time-invariant variables. The DP model is represented by differential equations of different DPs, while the GDQ model is represented by differential equations of multiple averaged dq-frame variables for ac variables and multiple DPs for dc variables. Theoretically, the number of DPs or averaged dq-frame variables can be of infinite order. In practical modeling, the model adequacy can be ensured by truncating the system considering dominant harmonic orders.

B. SMALL-SIGNAL LINEARIZATION

Given the equilibria representation, the small-signal model can be derived by Taylor series expansion applied to the nonlinear dynamic system [27], i.e.,

$$\dot{x} = f(x, u) = f(x_0, u_0) + \frac{\partial f}{\partial x}\Big|_{\substack{x=x_0 \\ u=u_0}} (x - x_0)$$

$$+ \frac{\partial f}{\partial u}\Big|_{\substack{x=x_0 \\ u=u_0}} (u - u_0) + R(x - x_0, u - u_0). \tag{8}$$

Eq. (8) applies to either real-valued or complex-valued equations, provided that those partial derivatives exist. By neglecting the higher-order derivatives, i.e., $R(x-x_0, u-u_0)$,

a small-signal model can be obtained as

$$\underbrace{f(x, u) - f(x_0, u_0)}_{\Delta f(x,u)}$$

$$\approx \underbrace{\frac{\partial f}{\partial x}\Big|_{\substack{x=x_0 \\ u=u_0}}}_{A} \underbrace{(x - x_0)}_{\Delta x} + \underbrace{\frac{\partial f}{\partial u}\Big|_{\substack{x=x_0 \\ u=u_0}}}_{B} \underbrace{(u - u_0)}_{\Delta u}. \tag{9}$$

This linearization applies to both time-varying and time-invariant systems. If the system equilibrium is time-periodic, represented by $x_0(t)$ and $u_0(t)$, the linearization yields an LTP system, whose state-space model is given by

$$\Delta \dot{x} = A(t)\, \Delta x + B(t)\, \Delta u$$

$$\Delta y = C(t)\, \Delta x + D(t)\, \Delta u, \tag{10}$$

where the "Δ" before signals will be neglected in the following small-signal models for simplicity. The resulted coefficients in (10) are all T-periodic, which can be represented by Fourier series, e.g.,

$$A(t) = \sum_k A_k e^{jk\omega_s t}, \tag{11}$$

where $\omega_s = 2\pi/T$, and similar for $B(t)$, $C(t)$, and $D(t)$. The LTP system builds the basis for the HSS modeling.

As for the DP or GDQ modeling, since the system equilibria are represented by time-invariant variables, i.e., the Fourier coefficients (DPs) or the averaged multiple dq-frame variables, the linearization yields an LTI system. Thus, the coefficients, A, B, C and D, are all constant.

It is noted that the DPs or GDQ variables can be more general concepts that include both the steady-state operating points and the small-signal dynamics, which characterize nonlinear behaviors. However, the linearized DP or GDQ model only characterizes the first-order small-signal dynamics in DPs or GDQ variables.

C. FREQUENCY-DOMAIN MODELING

The linearized time-domain model can be further derived in the frequency domain, which allows for using transfer functions to represent the system input-output dynamics.

The HSS modeling directly derives the frequency-domain representation of an LTP system in the state-space form, based on which the HTF can be derived to capture the system input-output dynamics in a similar manner to the LTI state-space analysis. The small-signal dynamics of the LTP system can be characterized by introducing the exponential function e^{st} to time-periodic signals, where $s \in \mathbb{C}$ represents any frequency-dependent dynamic, yielding the exponentially modulated periodic (EMP) signal [26] as

$$x = e^{st} \sum_k x_k e^{jk\omega_s t}. \tag{12}$$

It is worth noting that for an LTP system, its input and output responses can always be represented by such EMP signals. This is in analogous to that the input and output responses for an LTI system can always be represented by the form of $\Delta x e^{st}$,
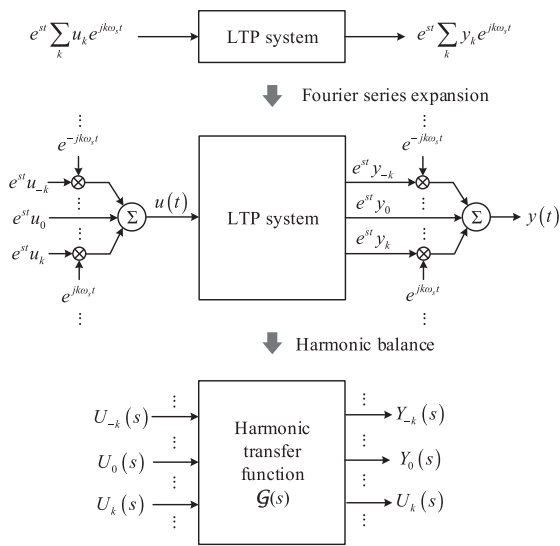
FIGURE 2. The frequency response of an LTP system represented by the harmonic transfer function.

namely a spiral vector [45]. In such a way, the frequency domain model of the LTP system can be derived based on Fourier series expansion and harmonic balance [35], as shown in Fig. 2. The harmonic transfer function (HTF) establishes a linear mapping between the Fourier coefficients of the input and output signals.

As for the DP and GDQ models, their linearized models are already LTI. Further Laplace transformations can be used to derive the frequency domain models. Alternatively, the frequency-domain model of an LTI system can be derived using spiral vectors [45], i.e., $\Delta x e^{st}$. With this approach, the frequency-dependent dynamics are introduced by the exponential function e^{st} modulated with time-invariant variables. This is in principle similar to the derivation of frequency-domain models for LTP systems using EMP signals.

III. UNIFIED MODELING FRAMEWORK
A unified modeling framework is proposed for ac power electronic systems. Since the ac system modeling focuses on the frequency couplings caused by converter control and system operating conditions, the averaged model that neglects the switching dynamics is assumed. The impacts of the Clark transformation and the real-to-complex transformation are considered, thus, the unified framework is developed by starting from the same averaged model represented in the $\alpha\beta$ frame using complex variables, as shown in Fig. 3. The HSS modeling, DP modeling and GDQ modeling are all involved in Fig. 3. Illustrations of the mathematical relationships among these methods are detailed in Parts A-C. Further discussions and recommendations are provided in Part D.

A. RELATIONSHIP BETWEEN HSS AND DP MODELING
The HSS model is derived by linearization first and Fourier series expansion next. The DP modeling yields the LTI model by Fourier series expansion first using GA operators and linearization next. Although they apply the linearization in different sequences, the derived models are essentially equivalent, since they use the same orthogonal basis, i.e., the basis of Fourier series. The GA operator used for DP modeling realizes the Fourier series expansion in the time domain, which is essentially a linear operator, as it satisfies the superposition principle. It is implied that this transformation can be flexibly exchanged with the linearization. In other words, the linearized DP model can be alternatively derived by applying the GA operators to the LTP model.

On the other hand, the HSS modeling and DP modeling result in model representations in different domains. The HSS model only represents the frequency-domain model of an LTP system, while the linearized DP model is usually represented in the time domain. Although represented in different domains, the HSS model and the DP model both use the time-invariant Fourier coefficients as input and output variables. If the linearized DP model is further derived in the frequency domain, it becomes the HSS model, which can be realized by the Laplace transformation [39] or using the spiral vector theory [45]. It is worth noting that if the HSS model is derived by GA operators applied to the LTP model first and spiral vectors applied to the linearized DP model next, it is in principle similar to the EMP signal-based HSS modeling yet follows a different sequence in modeling steps:

- The GA operators realize the Fourier series expansion first and the spiral vectors introduce the exponential function next;
- The EMP signal-based HSS modeling introduces the exponential function first and conducts the Fourier series expansion next.

B. RELATIONSHIP BETWEEN DP AND GDQ MODELING
As introduced in Section II, the DP modeling and GDQ modeling apply different transformations to realize the time-invariant representations of the system, and then perform the linearization around the time-invariant equilibria. Thus, their mathematical relationship lies in the relationship of the used transformations.

Since the GDQ model is derived by the GDQ transformation and SSA, as shown in (5) and (6), the two transformations can be combined and represented by integral operators, which yield the k-th averaged dq-frame variables denoted by

$$\mathbf{x}_{dqk} = \frac{1}{T} \int_{t-T}^{t} \mathbf{x}_{\alpha\beta} e^{-j(k\omega_s t + \varphi_k)} d\tau$$

$$\mathbf{x}_{dqk}^* = \frac{1}{T} \int_{t-T}^{t} \mathbf{x}_{\alpha\beta}^* e^{j(k\omega_s t + \varphi_k)} d\tau. \tag{13}$$

The integral operators in (13) are also linear transformations and apply to both large signals and small signals. Compared with the GA operators, additional exponential functions related to the initial phases are involved, where φ_k represents the initial phase used in the k-th dq transformation. It is thus indicated that the GDQ model can be transformed from the
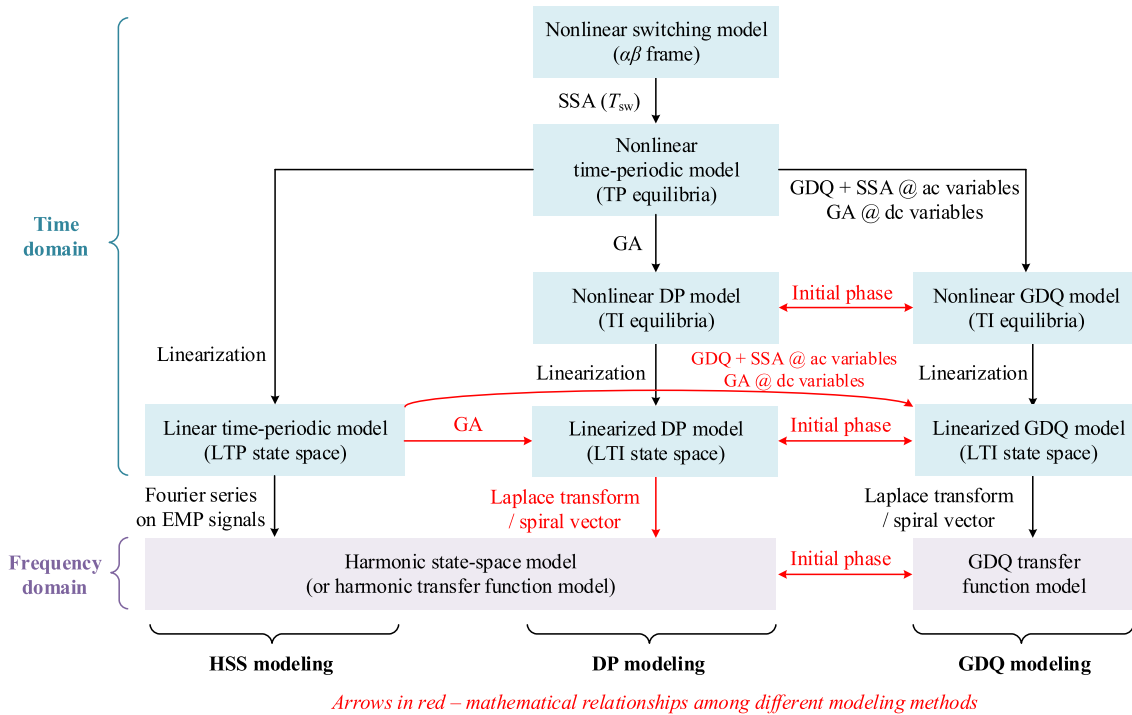
FIGURE 3. Unified modeling framework of HSS modeling, DP modeling and GDQ modeling for three-phase ac systems.

DP model through an initial-phase rotation,

$$
\begin{bmatrix} \mathbf{x}_{dqk} \\ \mathbf{x}^*_{dqk} \end{bmatrix} = \begin{bmatrix} e^{-j\varphi_k} & \\ & e^{j\varphi_k} \end{bmatrix} \begin{bmatrix} \langle \mathbf{x}_{\alpha\beta} \rangle_k \\ \langle \mathbf{x}^*_{\alpha\beta} \rangle_k \end{bmatrix}. \tag{14}
$$

The initial phase impact in the GDQ modeling was not discussed in previous works [40], [41], since the modeling was considered for a single converter system. When the system is linearized around the local steady-state dq frames of the converter system, the modeling can be simplified by selecting a time reference properly, such that the initial phase is assumed to be zero. However, the initial phase impact needs to be considered if a system includes multiple converters. In such cases, converters are interconnected through line impedances, and the initial phases of the converter terminal voltages are not equal generally due to the power flows. Each linearized converter model has to be transformed into common dq frames, and such initial phase rotations are inevitable [8].

C. RELATIONSHIP BETWEEN HSS AND GDQ MODELING

Considering the relationships between the HSS and DP modeling and between the DP and GDQ modeling, it can be easily deduced that the linearized GDQ model can also be derived from the LTP model based on the GDQ transformation and SSA, and the HSS model can be derived from the GDQ frequency-domain model considering the initial phase rotation.

D. DISCUSSIONS AND RECOMMENDATIONS

The unified modeling framework indicates that the transformation and linearization can be exchanged flexibly in the modeling process. No matter the linearization is done around the time-periodic trajectories or the time-invariant points, the same model can be resulted as long as the same transformations are used. The HSS modeling benefits in an efficient modeling since the time-periodic coefficients can be easily represented by the Toeplitz matrices using Fourier coefficients in the frequency domain [26], which can be solved numerically by applying the discrete Fourier transformation (DFT) to time-domain waveforms. Thus, the Toeplitz matrices of time-periodic variables can also be used to establish DP or GDQ models more efficiently based on numerical solutions.

It can be seen that the HSS model or the DP model is merely distinguished from the GDQ model considering an initial phase rotation. That is to say, the HSS model or the DP model can also be interpreted as a "multi-dq" frame model, since the variables in the HSS or DP model are Fourier coefficients, which are essentially dq-frame variables of one phasor at a specific harmonic frequency. This is why these methods are essentially equivalent and can be unified for the ac system modeling. Compared with the GDQ modeling, HSS or DP modeling does not need to consider the initial phases deliberately in the modeling process, since the initial phases are inherently included in the Fourier coefficients when the Toeplitz matrices of time-periodic variables are calculated based on a common time reference.

The mathematical relationships of different modeling methods are derived assuming that the model order can be infinite,
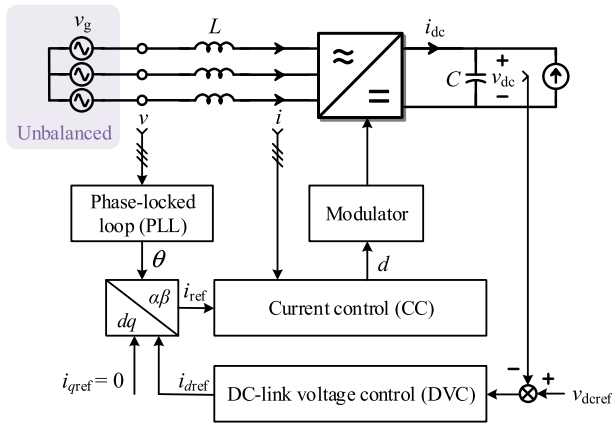
FIGURE 4. Studied three-phase voltage-source converter under unbalanced grids.

TABLE 1. VSC Parameters

Parameters	Symbols	Values
Grid voltage	V_p	1.0 p.u. (200 V)
	V_n	0.5 p.u.
Fundamental angular frequency	ω_s	$2\pi \cdot 50$ rad/s
Inverter L filter	L	2 mH
DC voltage	V_{dc}	600 V
DC current	I_{dc}	3 A
DC-side capacitance	C	0.45 mF
q-axis current reference	I_q	0 A
Current PR Controller	K_{pi}	12 Ω
	K_{ri}	1500 Ω/s
PLL PI controller and notch filter damping factor	K_{ppll}	0.58 rad/(s·V)
	K_{ipll}	27.2 rad/(s²·V)
	D_p	0.707
DC-link voltage controller	K_{pdvc}	0.5 S
	K_{idvc}	20 S/s

i.e, $k \rightarrow \infty$. However, in practical implementations, a finite k needs to be selected to truncate the HSS (or HTF) model, the DP model, or the GDQ model. The DP or GDQ modeling considers the truncation by selecting the order of transformations, whereas the HSS modeling considers the truncation by selecting the order of HTFs. They finally result in the same truncation effects, since these models are equivalent to each other. However, the truncation order can be unclear for the DP or GDQ modeling at the beginning when defining the transformations. Thus, it is recommended to assume an unknown k to conduct the DP or GDQ modeling first, and finally determines the value of k based on the system steady-state analysis and the resulted Toeplitz matrices in the model. This way of model truncation will be considered and discussed in the following case study.

FIGURE 5. Different ways to the linearized modeling of the converter system.

IV. CASE STUDY

To verify the unified modeling framework, the linearized modeling of a three-phase converter system is conducted under unbalanced grid conditions. The relationships among different modeling methods are firstly verified on the converter power stage by mathematical proofs and time-domain simulations, where the nonlinearity introduced by converter ac-dc modulation is studied. Since different modeling methods can yield a unified HTF model in the frequency domain, the converter HTF model considering the closed-loop control dynamics is further derived, where the nonlinearity caused by Park and inverse Park transformations in converter control is considered. The unified HTF model of the converter is finally validated by frequency scan in experiments.

A. SYSTEM DESCRIPTION

Fig. 4 shows the three-phase converter under study, which is operating with unbalanced three-phase voltages. The converter has the current control (CC), the phase-locked loop (PLL) and the dc-link voltage control (DVC). The CC is implemented in $\alpha\beta$ frame with proportional + resonant (PR)

controllers. The PLL adopts a notch-filtered synchronous-reference-frame PLL, in order to filter out the negative-sequence voltage components for synchronization. The DVC adopts a proportional + integral (PI) controller. The circuit and control parameters are listed in Table 1.

The converter system has multiple nonlinear parts, including the ac-dc modulation in power stage and the Park / inverse Park transformations in converter control. To conduct the modular modeling, the converter system can be partitioned into several subsystems. The converter power stage, the PLL and the DVC are nonlinear subsystems, while the CC and the time delay are linear subsystems. The linearized modeling can be applied for each nonlinear subsystem.

B. CONVERTER POWER-STAGE MODELING TO VERIFY MATHEMATICAL RELATIONSHIPS

To verify the relationships of different modeling methods, the converter power stage is modeled first. Different ways of modeling are adopted, as shown in Fig. 5. The dashed arrows show how the HSS model and the linearized DP model are

derived in the conventional ways. To highlight the mathematical relationships of different modeling methods, the following derivations do not adopt the conventional ways. Instead, Way 1 and Way 2 are used, which follow the blue arrows and red arrows, respectively.

At the beginning, the converter system is modeled through an SSA operator over the switching period (T_{sw}). The averaged model can be derived in the $\alpha\beta$ frame using complex variables, which is provided as

$$
\begin{bmatrix} \mathbf{v}_{\alpha\beta} \\ \mathbf{v}_{\alpha\beta}^* \end{bmatrix} = L \frac{\mathrm{d}}{\mathrm{d}t} \begin{bmatrix} \mathbf{i}_{\alpha\beta} \\ \mathbf{i}_{\alpha\beta}^* \end{bmatrix} + v_{\text{dc}} \begin{bmatrix} \mathbf{d}_{\alpha\beta} \\ \mathbf{d}_{\alpha\beta}^* \end{bmatrix}
$$
$$
C \frac{\mathrm{d}v_{\text{dc}}}{\mathrm{d}t} = \begin{bmatrix} \frac{1}{2}\mathbf{d}_{\alpha\beta}^* & \frac{1}{2}\mathbf{d}_{\alpha\beta} \end{bmatrix} \begin{bmatrix} \mathbf{i}_{\alpha\beta} \\ \mathbf{i}_{\alpha\beta}^* \end{bmatrix} \tag{15}
$$

Eq. (15) is nonlinear and time-periodic. The nonlinearity comes from the modulation between the duty cycle vector ($[\mathbf{d}_{\alpha\beta}, \mathbf{d}_{\alpha\beta}^*]^{\mathrm{T}}$) and the dc voltage ($v_{\text{dc}}$) or the ac current vector ($[\mathbf{i}_{\alpha\beta}, \mathbf{i}_{\alpha\beta}^*]^{\mathrm{T}}$).

1) WAY 1 (FOLLOWING BLUE ARROWS IN FIG. 5)
Linearizing (15) yields the LTP model as

$$
\begin{bmatrix} \mathbf{v}_{\alpha\beta} \\ \mathbf{v}_{\alpha\beta}^* \end{bmatrix} = L \frac{\mathrm{d}}{\mathrm{d}t} \begin{bmatrix} \mathbf{i}_{\alpha\beta} \\ \mathbf{i}_{\alpha\beta}^* \end{bmatrix} + V_{\text{dc}}(t) \begin{bmatrix} \mathbf{d}_{\alpha\beta} \\ \mathbf{d}_{\alpha\beta}^* \end{bmatrix} + \begin{bmatrix} \mathbf{D}_{\alpha\beta}(t) \\ \mathbf{D}_{\alpha\beta}^*(t) \end{bmatrix} v_{\text{dc}}
$$
$$
C \frac{\mathrm{d}v_{\text{dc}}}{\mathrm{d}t} = \frac{1}{2} \begin{pmatrix} \mathbf{D}_{\alpha\beta}(t)\mathbf{i}_{\alpha\beta}^* + \mathbf{D}_{\alpha\beta}^*(t)\mathbf{i}_{\alpha\beta} \\ + \mathbf{I}_{\alpha\beta}^*(t)\mathbf{d}_{\alpha\beta} + \mathbf{I}_{\alpha\beta}(t)\mathbf{d}_{\alpha\beta}^* \end{pmatrix}, \tag{16}
$$

where the steady-state trajectories are represented by the $\alpha\beta$-frame variables ($\mathbf{D}_{\alpha\beta}(t)$, $\mathbf{D}_{\alpha\beta}^*(t)$, $\mathbf{I}_{\alpha\beta}(t)$, $\mathbf{I}_{\alpha\beta}^*(t)$) and $V_{\text{dc}}(t)$.

Under the unbalanced grid condition, the $\alpha\beta$-frame variables and the dc voltage may have multiple harmonic components. Thus, the GA operators can be further used to derive the DP model, which yields

$$
\begin{bmatrix} \langle\mathbf{v}_{\alpha\beta}\rangle \\ \langle\mathbf{v}_{\alpha\beta}^*\rangle \end{bmatrix} = L \frac{\mathrm{d}}{\mathrm{d}t} \begin{bmatrix} \langle\mathbf{i}_{\alpha\beta}\rangle \\ \langle\mathbf{i}_{\alpha\beta}^*\rangle \end{bmatrix} + L\mathcal{N} \begin{bmatrix} \langle\mathbf{i}_{\alpha\beta}\rangle \\ \langle\mathbf{i}_{\alpha\beta}^*\rangle \end{bmatrix}
$$
$$
+ \mathcal{V}_{\text{dc}} \begin{bmatrix} \langle\mathbf{d}_{\alpha\beta}\rangle \\ \langle\mathbf{d}_{\alpha\beta}^*\rangle \end{bmatrix} + \begin{bmatrix} \mathcal{D}_{\alpha\beta} & \\ & \mathcal{D}_{\alpha\beta}^* \end{bmatrix} \begin{bmatrix} \langle v_{\text{dc}}\rangle \\ \langle v_{\text{dc}}\rangle^* \end{bmatrix}
$$
$$
C \frac{\mathrm{d}}{\mathrm{d}t} \langle v_{\text{dc}}\rangle + C\mathcal{N}\langle v_{\text{dc}}\rangle = \frac{1}{2}\mathcal{D}_{\alpha\beta}\langle\mathbf{i}_{\alpha\beta}^*\rangle + \frac{1}{2}\mathcal{I}_{\alpha\beta}\langle\mathbf{d}_{\alpha\beta}^*\rangle
$$
$$
+ \frac{1}{2}\mathcal{D}_{\alpha\beta}^*\langle\mathbf{i}_{\alpha\beta}\rangle + \frac{1}{2}\mathcal{I}_{\alpha\beta}^*\langle\mathbf{d}_{\alpha\beta}\rangle, \tag{17}
$$

where $\langle\mathbf{v}_{\alpha\beta}\rangle = \begin{bmatrix} \langle\mathbf{v}_{\alpha\beta}\rangle_{-k} \\ \vdots \\ \langle\mathbf{v}_{\alpha\beta}\rangle_0 \\ \vdots \\ \langle\mathbf{v}_{\alpha\beta}\rangle_{+k} \end{bmatrix} = \begin{bmatrix} \langle v_\alpha\rangle_{-k} + j\langle v_\beta\rangle_{-k} \\ \vdots \\ \langle v_\alpha\rangle_0 + j\langle v_\beta\rangle_0 \\ \vdots \\ \langle v_\alpha\rangle_{+k} + j\langle v_\beta\rangle_{+k} \end{bmatrix}$,

$$
\langle\mathbf{v}_{\alpha\beta}^*\rangle = \begin{bmatrix} \langle\mathbf{v}_{\alpha\beta}^*\rangle_{-k} \\ \vdots \\ \langle\mathbf{v}_{\alpha\beta}^*\rangle_0 \\ \vdots \\ \langle\mathbf{v}_{\alpha\beta}^*\rangle_{+k} \end{bmatrix} = \begin{bmatrix} \langle v_\alpha\rangle_{-k} - j\langle v_\beta\rangle_{-k} \\ \vdots \\ \langle v_\alpha\rangle_0 - j\langle v_\beta\rangle_0 \\ \vdots \\ \langle v_\alpha\rangle_{+k} - j\langle v_\beta\rangle_{+k} \end{bmatrix}, \text{ such that}
$$

$\langle\mathbf{v}_{\alpha\beta}^*\rangle_{+k} = \left(\langle\mathbf{v}_{\alpha\beta}\rangle_{-k}\right)^*$ and similar for other variables

$\mathcal{N} = diag\{-jk\omega_s, \cdots, 0, \cdots, jk\omega_s\}$ is a diagonal matrix. $\mathcal{V}_{\text{dc}}, \mathcal{D}_{\alpha\beta}, \mathcal{D}_{\alpha\beta}^*, \mathcal{I}_{\alpha\beta}, \mathcal{I}_{\alpha\beta}^*$ are represented by Toeplitz matrices of the steady-state trajectories, whose general form is denoted by

$$
\mathcal{X} = \begin{bmatrix} \ddots & & & & \reflectbox{$\ddots$} \\ & X_0 & X_{-1} & X_{-2} & \\ & X_1 & X_0 & X_{-1} & \\ & X_2 & X_1 & X_0 & \\ \reflectbox{$\ddots$} & & & & \ddots \end{bmatrix} \text{ for } X(t) = \sum_k X_k e^{jk\omega_s t}. \tag{18}
$$

When the variable is complex, its Toeplitz matrix can be calculated by $\mathcal{X}_{\alpha\beta} = \mathcal{X}_\alpha + j\mathcal{X}_\beta$, $\mathcal{X}_{\alpha\beta}^* = \mathcal{X}_\alpha - j\mathcal{X}_\beta$.

The DP model in (17) is an LTI model in the time domain. It can be further transformed into the frequency domain via the Laplace transformation or spiral vectors [45], yielding

$$
\begin{bmatrix} \langle\mathbf{v}_{\alpha\beta}\rangle(s) \\ \langle\mathbf{v}_{\alpha\beta}^*\rangle(s) \end{bmatrix} = sL \begin{bmatrix} \langle\mathbf{i}_{\alpha\beta}\rangle(s) \\ \langle\mathbf{i}_{\alpha\beta}^*\rangle(s) \end{bmatrix} + L\mathcal{N} \begin{bmatrix} \langle\mathbf{i}_{\alpha\beta}\rangle(s) \\ \langle\mathbf{i}_{\alpha\beta}^*\rangle(s) \end{bmatrix}
$$
$$
+ \mathcal{V}_{\text{dc}} \begin{bmatrix} \langle\mathbf{d}_{\alpha\beta}\rangle(s) \\ \langle\mathbf{d}_{\alpha\beta}^*\rangle(s) \end{bmatrix} + \begin{bmatrix} \mathcal{D}_{\alpha\beta} & \\ & \mathcal{D}_{\alpha\beta}^* \end{bmatrix} \begin{bmatrix} \langle v_{\text{dc}}\rangle(s) \\ \langle v_{\text{dc}}\rangle^*(s) \end{bmatrix}
$$
$$
sC\langle v_{\text{dc}}\rangle(s) + C\mathcal{N}\langle v_{\text{dc}}\rangle(s) = \frac{1}{2}\mathcal{D}_{\alpha\beta}\langle\mathbf{i}_{\alpha\beta}^*\rangle(s)
$$
$$
+ \frac{1}{2}\mathcal{I}_{\alpha\beta}\langle\mathbf{d}_{\alpha\beta}^*\rangle(s)
$$
$$
+ \frac{1}{2}\mathcal{D}_{\alpha\beta}^*\langle\mathbf{i}_{\alpha\beta}\rangle(s) + \frac{1}{2}\mathcal{I}_{\alpha\beta}^*\langle\mathbf{d}_{\alpha\beta}\rangle(s). \tag{19}
$$

It can be seen that Eq. (19) is essentially an HTF model represented with complex variables, which can be easily written in the HSS form with simple reformulations. Thus, the relationship between the HSS modeling and DP modeling has been proved.

2) WAY 2 (FOLLOWING RED ARROWS IN FIG. 5)
The GDQ model can be derived from (15) based on the GDQ transformation plus the SSA for ac variables and the GA for dc variables, which first yields the nonlinear GDQ model as (20) shown at the bottom of the next page.

It can be seen that the initial-phase related rotations are involved in the nonlinear parts of the differential equations. Then, further linearization can be conducted, yielding the

linearized GDQ model as

$$
\begin{bmatrix} \mathbf{v}_{dq-k} \\ \vdots \\ \mathbf{v}_{dq0} \\ \vdots \\ \mathbf{v}_{dqk} \end{bmatrix} = L\frac{\mathrm{d}}{\mathrm{d}t}\begin{bmatrix} \mathbf{i}_{dq-k} \\ \vdots \\ \mathbf{i}_{dq0} \\ \vdots \\ \mathbf{i}_{dqk} \end{bmatrix} + L\mathcal{N}\begin{bmatrix} \mathbf{i}_{dq-k} \\ \vdots \\ \mathbf{i}_{dq0} \\ \vdots \\ \mathbf{i}_{dqk} \end{bmatrix}
$$

$$
+ Q\mathcal{V}_{\mathrm{dc}}Q^{-1}\begin{bmatrix} \mathbf{d}_{dq-k} \\ \vdots \\ \mathbf{d}_{dq0} \\ \vdots \\ \mathbf{d}_{dqk} \end{bmatrix} + Q\mathcal{D}_{\alpha\beta}\begin{bmatrix} \langle v_{\mathrm{dc}}\rangle_{-k} \\ \vdots \\ \langle v_{\mathrm{dc}}\rangle_0 \\ \vdots \\ \langle v_{\mathrm{dc}}\rangle_{+k} \end{bmatrix} \quad (21\mathrm{a})
$$

$$
\begin{bmatrix} \mathbf{v}_{dqk}^* \\ \vdots \\ \mathbf{v}_{dq0}^* \\ \vdots \\ \mathbf{v}_{dq-k}^* \end{bmatrix} = L\frac{\mathrm{d}}{\mathrm{d}t}\begin{bmatrix} \mathbf{i}_{dqk}^* \\ \vdots \\ \mathbf{i}_{dq0}^* \\ \vdots \\ \mathbf{i}_{dq-k}^* \end{bmatrix} + L\mathcal{N}\begin{bmatrix} \mathbf{i}_{dqk}^* \\ \vdots \\ \mathbf{i}_{dq0}^* \\ \vdots \\ \mathbf{i}_{dq-k}^* \end{bmatrix}
$$

$$
+ R\mathcal{V}_{\mathrm{dc}}R^{-1}\begin{bmatrix} \mathbf{d}_{dqk}^* \\ \vdots \\ \mathbf{d}_{dq0}^* \\ \vdots \\ \mathbf{d}_{dq-k}^* \end{bmatrix} + R\mathcal{D}_{\alpha\beta}^*\begin{bmatrix} \langle v_{\mathrm{dc}}\rangle_k \\ \vdots \\ \langle v_{\mathrm{dc}}\rangle_0 \\ \vdots \\ \langle v_{\mathrm{dc}}\rangle_{-k} \end{bmatrix} \quad (21\mathrm{b})
$$

$$
C\frac{\mathrm{d}}{\mathrm{d}t}\begin{bmatrix} \langle v_{\mathrm{dc}}\rangle_{-k} \\ \vdots \\ \langle v_{\mathrm{dc}}\rangle_0 \\ \vdots \\ \langle v_{\mathrm{dc}}\rangle_{+k} \end{bmatrix} + C\mathcal{N}\begin{bmatrix} \langle v_{\mathrm{dc}}\rangle_{-k} \\ \vdots \\ \langle v_{\mathrm{dc}}\rangle_0 \\ \vdots \\ \langle v_{\mathrm{dc}}\rangle_{+k} \end{bmatrix} = \frac{1}{2}\mathcal{D}_{\alpha\beta}^*Q^{-1}\begin{bmatrix} \mathbf{i}_{dq-k} \\ \vdots \\ \mathbf{i}_{dq0} \\ \vdots \\ \mathbf{i}_{dqk} \end{bmatrix}
$$

$$
+ \frac{1}{2}\mathcal{I}_{\alpha\beta}^*Q^{-1}\begin{bmatrix} \mathbf{d}_{dq-k} \\ \vdots \\ \mathbf{d}_{dq0} \\ \vdots \\ \mathbf{d}_{dqk} \end{bmatrix} + \frac{1}{2}\mathcal{D}_{\alpha\beta}Q\begin{bmatrix} \mathbf{i}_{dq-k}^* \\ \vdots \\ \mathbf{i}_{dq0}^* \\ \vdots \\ \mathbf{i}_{dqk}^* \end{bmatrix}
$$

$$
+ \frac{1}{2}\mathcal{I}_{\alpha\beta}Q\begin{bmatrix} \mathbf{d}_{dq-k}^* \\ \vdots \\ \mathbf{d}_{dq0}^* \\ \vdots \\ \mathbf{d}_{dqk}^* \end{bmatrix} \quad (21\mathrm{c})
$$

where Q and R are initial-phase rotation matrices defined as

$$
Q = diag\left\{e^{-j\varphi_{-k}}, \cdots, e^{-j\varphi_0}, \cdots, e^{-j\varphi_k}\right\} \quad (22)
$$

$$
R = diag\left\{e^{j\varphi_k}, \cdots, e^{j\varphi_0}, \cdots, e^{j\varphi_{-k}}\right\} \quad (23)
$$

It can be derived that if all the ac variables in (21a) and (21b) are multiplied by Q^{-1} and R^{-1}, respectively, the GDQ model is transformed into the DP model as shown in (17).

$$
\begin{bmatrix} \mathbf{v}_{dq-k} \\ \vdots \\ \mathbf{v}_{dq0} \\ \vdots \\ \mathbf{v}_{dqk} \end{bmatrix} = L\frac{\mathrm{d}}{\mathrm{d}t}\begin{bmatrix} \mathbf{i}_{dq-k} \\ \vdots \\ \mathbf{i}_{dq0} \\ \vdots \\ \mathbf{i}_{dqk} \end{bmatrix} + L\mathcal{N}\begin{bmatrix} \mathbf{i}_{dq-k} \\ \vdots \\ \mathbf{i}_{dq0} \\ \vdots \\ \mathbf{i}_{dqk} \end{bmatrix} + \begin{bmatrix} \sum_m \langle v_{\mathrm{dc}}\rangle_m e^{-j(\varphi_{-k}-\varphi_{-k-m})}\mathbf{d}_{dq,-k-m} \\ \vdots \\ \sum_m \langle v_{\mathrm{dc}}\rangle_m e^{-j(\varphi_0-\varphi_{-m})}\mathbf{d}_{dq,-m} \\ \vdots \\ \sum_m \langle v_{\mathrm{dc}}\rangle_m e^{-j(\varphi_k-\varphi_{k-m})}\mathbf{d}_{dq,k-m} \end{bmatrix}, \quad (20\mathrm{a})
$$

$$
\begin{bmatrix} \mathbf{v}_{dqk}^* \\ \vdots \\ \mathbf{v}_{dq0}^* \\ \vdots \\ \mathbf{v}_{dq-k}^* \end{bmatrix} = L\frac{\mathrm{d}}{\mathrm{d}t}\begin{bmatrix} \mathbf{i}_{dqk}^* \\ \vdots \\ \mathbf{i}_{dq0}^* \\ \vdots \\ \mathbf{i}_{dq-k}^* \end{bmatrix} + L\mathcal{N}\begin{bmatrix} \mathbf{i}_{dqk}^* \\ \vdots \\ \mathbf{i}_{dq0}^* \\ \vdots \\ \mathbf{i}_{dq-k}^* \end{bmatrix} + \begin{bmatrix} \sum_m \langle v_{\mathrm{dc}}\rangle_{-m} e^{j(\varphi_k-\varphi_{k-m})}\mathbf{d}_{dq,k-m}^* \\ \vdots \\ \sum_m \langle v_{\mathrm{dc}}\rangle_{-m} e^{j(\varphi_0-\varphi_{-m})}\mathbf{d}_{dq,-m}^* \\ \vdots \\ \sum_m \langle v_{\mathrm{dc}}\rangle_{-m} e^{j(\varphi_{-k}-\varphi_{-k-m})}\mathbf{d}_{dq,-k-m}^* \end{bmatrix}, \quad (20\mathrm{b})
$$

$$
C\frac{\mathrm{d}}{\mathrm{d}t}\begin{bmatrix} \langle v_{\mathrm{dc}}\rangle_{-k} \\ \vdots \\ \langle v_{\mathrm{dc}}\rangle_0 \\ \vdots \\ \langle v_{\mathrm{dc}}\rangle_{+k} \end{bmatrix} = \frac{1}{2}\begin{bmatrix} \sum_m \mathbf{d}_{dq,-m}^*\mathbf{i}_{dq,m-k}e^{-j(\varphi_{-m}-\varphi_{m-k})} \\ \vdots \\ \sum_m \mathbf{d}_{dq,-m}^*\mathbf{i}_{dq,m}e^{-j(\varphi_{-m}-\varphi_m)} \\ \vdots \\ \sum_m \mathbf{d}_{dq,-m}^*\mathbf{i}_{dq,m+k}e^{-j(\varphi_{-m}-\varphi_{m+k})} \end{bmatrix} + \frac{1}{2}\begin{bmatrix} \sum_m \mathbf{d}_{dq,-m}\mathbf{i}_{dq,m-k}^*e^{j(\varphi_{-m}-\varphi_{m-k})} \\ \vdots \\ \sum_m \mathbf{d}_{dq,-m}\mathbf{i}_{dq,m}^*e^{j(\varphi_{-m}-\varphi_m)} \\ \vdots \\ \sum_m \mathbf{d}_{dq,-m}\mathbf{i}_{dq,m+k}^*e^{j(\varphi_{-m}-\varphi_{m+k})} \end{bmatrix} \quad (20\mathrm{c})
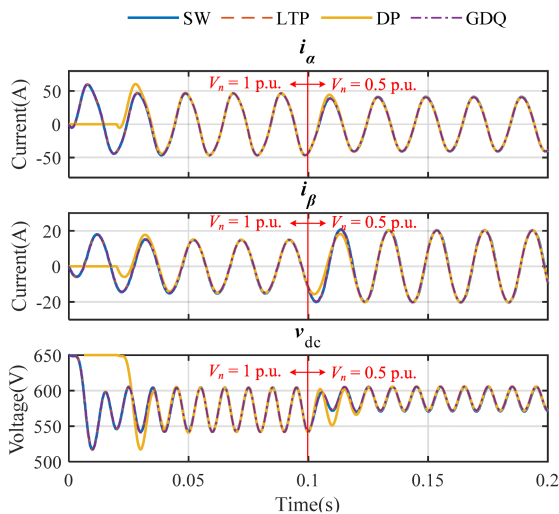$$

FIGURE 6. Open-loop validation among different models for a three-phase converter in unbalanced grids.

FIGURE 7. Mathematical relationship validation between the DP and GDQ models.

Thus, the relationship between the DP and GDQ modeling has been proved.

3) TIME-DOMAIN VALIDATION

The mathematical relationship of these models are further validated by the time-domain electromagnetic transient (EMT) simulations in MATLAB/Simulink.

The switching (SW) model, the LTP model, the DP model and the GDQ model of the open-loop converter system are established, and the time-domain waveforms of the ac voltages, ac currents, and dc voltage are compared in Fig. 6. It is noted that although the DPs and GDQ variables are time-invariant, the original ac signals can be reconstructed by multiple DPs based on Fourier series summation and by multiple GDQ variables based on (7). At 0.1 s, the negative-sequence voltage steps from 1 p.u. to 0.5 p.u.. It is found that all the models agree with each other, such that mathematical relationships of the LTP model and the DP/GDQ model can be verified. The DP model has some time delay in the agreement, since the DPs are calculated by a moving averaging window.

To further verify the mathematical relationships between the DP model and the GDQ model, Fig. 7 compares different DPs and multiple GDQ variables considering the initial-phase rotation impacts. For easier plotting in the time domain, the real and imaginary parts of the complex-valued DPs and GDQ variables are calculated and compared. It can be seen that, after applying the initial phase rotation to the GDQ variables, the waveforms agree with the DPs.

C. CLOSED-LOOP MODELING TO VERIFY THE UNIFIED HTF MODEL

As the relationship of different modeling methods have been verified on the power stage model, the closed-loop modeling will focus on how to integrate control dynamics with the co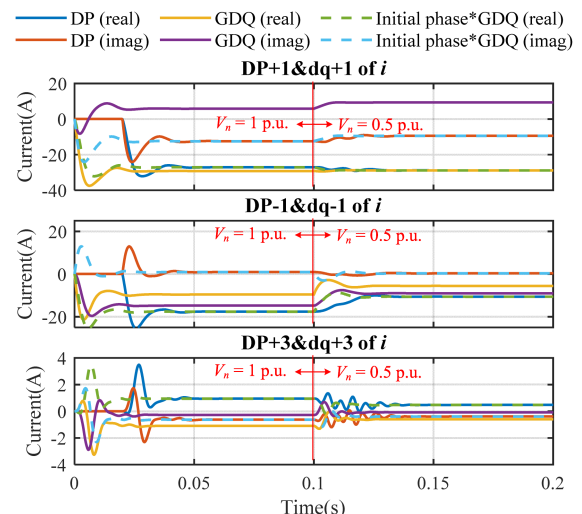nverter power stage to derive a unified HTF model. To facilitate a scalable closed-loop modeling, the models of converter power stage and different control loops are all derived using HTFs. Then, the closed-loop model can be depicted by interconnecting these subsystems according to the control structure. However, the interconnection of HTFs requires to truncate the HTFs with the same order, thus the truncation of HTFs will be discussed first.

1) VARIABLE REPRESENTATION FOR HTF ORDER REDUCTION

Different variable representations can make a difference in the HTF order selection. First, how find a minimum order for the HTF truncation is discussed, which can simplify the model validation by frequency scan.

As mentioned in Section III-D, the HTF truncation is influenced by the steady-state harmonics in the operating trajectories, which can be analyzed numerically based on the DFTs. The frequency-domain model of the converter power stage has been explicitly shown by (19). However, those ac and dc variable representations do not consider the inherent frequency coupling relationships in the converter system, which can result in a high HTF truncation order. It is seen that the HTFs of $\mathcal{V}_{dc}$, $\mathcal{D}_{\alpha\beta}$, $\mathcal{D}_{\alpha\beta}^*$, $\mathcal{I}_{\alpha\beta}$, $\mathcal{I}_{\alpha\beta}^*$ in (19) are calculated by the Toeplitz matrices of the steady-state trajectories in (16). According to the steady-state spectrum shown in Fig. 8(a), the ac variables, represented by $\mathbf{X}_{\alpha\beta}(t)$ and $\mathbf{X}_{\alpha\beta}^*(t)$ which can be either duty cycle or current, contain dominant harmonics up to $\pm 3 f_s$ under the unbalanced grid conditions. Since the fundamental frequency is f_s, high-order HTFs at least with the order of 7 are needed to characterize the dynamical impacts of grid unbalance.

To reduce the HTF truncation order, the inherent ac-dc frequency coupling relationship of converter systems can be considered in the variable representations. It has been revealed that the three-phase converter system can be represented by a three-port network, where any ac variables are represented by
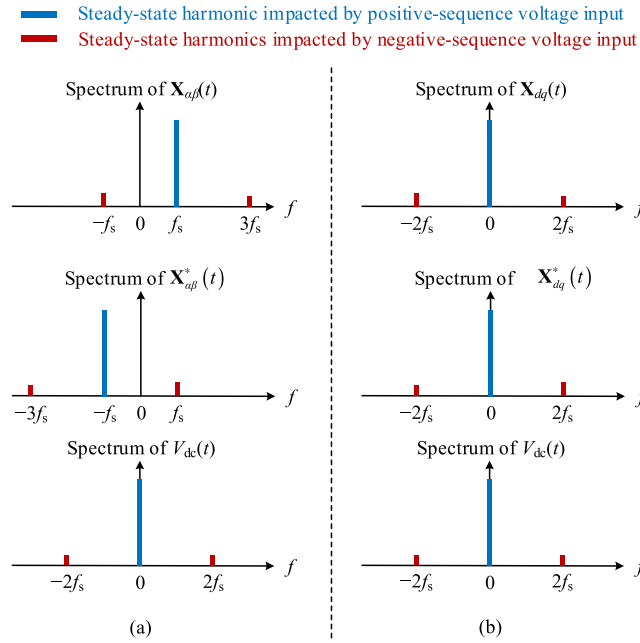
FIGURE 8. Harmonic spectra of steady-state trajectories under unbalanced grid conditions. (a) Variable representations without considering the ac-dc frequency coupling relationship; (b) Variable representations considering the ac-dc frequency coupling relationship.

$\mathbf{x}_{\alpha\beta}$, $e^{j2\theta_s}\mathbf{x}^*_{\alpha\beta}$, and any dc variable is denoted by $e^{j\theta_s}x_{\text{dc}}$ [12]. The use of exponential functions with complex variables can characterize the inherent frequency coupling dynamics in the converter system. With such variable representations, the LTP model of the converter power stage can be then modified from (16) as

$$\begin{bmatrix} \mathbf{v}_{\alpha\beta} \\ e^{j2\theta_s}\mathbf{v}^*_{\alpha\beta} \end{bmatrix} = \begin{bmatrix} L\frac{\mathrm{d}}{\mathrm{d}t} & \\ & e^{j2\theta_s}L\frac{\mathrm{d}}{\mathrm{d}t}e^{-j2\theta_s} \end{bmatrix} \begin{bmatrix} \mathbf{i}_{\alpha\beta} \\ e^{j2\theta_s}\mathbf{i}^*_{\alpha\beta} \end{bmatrix}$$
$$+ V_{\text{dc}}(t) \begin{bmatrix} \mathbf{d}_{\alpha\beta} \\ e^{j2\theta_s}\mathbf{d}^*_{\alpha\beta} \end{bmatrix} + \begin{bmatrix} \mathbf{D}_{dq}(t) \\ \mathbf{D}^*_{dq}(t) \end{bmatrix} e^{j\theta_s} v_{\text{dc}} \quad (24a)$$

$$e^{j\theta_s}C\frac{\mathrm{d}}{\mathrm{d}t}e^{-j\theta_s}\left(e^{j\theta_s}v_{\text{dc}}\right) = \frac{1}{2}\begin{bmatrix} \mathbf{D}^*_{dq}(t) & \mathbf{D}_{dq}(t) \end{bmatrix}\begin{bmatrix} \mathbf{i}_{\alpha\beta} \\ e^{j2\theta_s}\mathbf{i}^*_{\alpha\beta} \end{bmatrix}$$
$$+ \frac{1}{2}\begin{bmatrix} \mathbf{I}^*_{dq}(t) & \mathbf{I}_{dq}(t) \end{bmatrix}\begin{bmatrix} \mathbf{d}_{\alpha\beta} \\ e^{j2\theta_s}\mathbf{d}^*_{\alpha\beta} \end{bmatrix} \quad (24b)$$

It can be seen that the steady-state trajectories are currently represented by the positive-sequence dq-frame variables ($\mathbf{D}_{dq}(t)$, $\mathbf{D}^*_{dq}(t)$, $\mathbf{I}_{dq}(t)$, $\mathbf{I}^*_{dq}(t)$) and $V_{\text{dc}}(t)$. Consequently, the frequency domain model can be represented by HTFs as

$$\begin{bmatrix} \langle\mathbf{v}_{\alpha\beta}\rangle(s) \\ \langle\mathbf{v}^*_{\alpha\beta}\rangle(s-j2\omega_s) \end{bmatrix} = \begin{bmatrix} \mathbf{Z}_L(s) & \\ & \mathbf{Z}_L(s-j2\omega_s) \end{bmatrix}$$
$$\times \begin{bmatrix} \langle\mathbf{i}_{\alpha\beta}\rangle(s) \\ \langle\mathbf{i}^*_{\alpha\beta}\rangle(s-j2\omega_s) \end{bmatrix}$$

$$+ \mathcal{V}_{\text{dc}}\begin{bmatrix} \langle\mathbf{d}_{\alpha\beta}\rangle(s) \\ \langle\mathbf{d}^*_{\alpha\beta}\rangle(s-j2\omega_s) \end{bmatrix} + \begin{bmatrix} \mathcal{D}_{dq} & \\ & \mathcal{D}^*_{dq} \end{bmatrix}\langle v_{\text{dc}}\rangle(s-j\omega_s)$$
$$\quad (25a)$$

$$\mathbf{Y}_C(s-j\omega_s)\langle v_{\text{dc}}\rangle(s-j\omega_s)$$
$$= \frac{1}{2}\begin{bmatrix} \mathcal{D}^*_{dq} & \mathcal{D}_{dq} \end{bmatrix}\begin{bmatrix} \langle\mathbf{i}_{\alpha\beta}\rangle(s) \\ \langle\mathbf{i}^*_{\alpha\beta}\rangle(s-j2\omega_s) \end{bmatrix}$$
$$+ \frac{1}{2}\begin{bmatrix} \mathcal{I}^*_{dq} & \mathcal{I}_{dq} \end{bmatrix}\begin{bmatrix} \langle\mathbf{d}_{\alpha\beta}\rangle(s) \\ \langle\mathbf{d}^*_{\alpha\beta}\rangle(s-j2\omega_s) \end{bmatrix} \quad (25b)$$

where $\mathbf{Z}_L(s) = diag\{(s-jk\omega_s)L, \cdots, sL, \cdots, (s+jk\omega_s)L\}$ and $\mathbf{Y}_C(s) = diag\{(s-jk\omega_s)C, \cdots, sC, \cdots, (s+jk\omega_s)C\}$.

According to (24) and (25), the HTFs can be truncated based on harmonic spectra of the steady-state trajectories, i.e., $\mathbf{X}_{dq}(t)$, $\mathbf{X}^*_{dq}(t)$, and $V_{\text{dc}}(t)$, which are shown in Fig. 8(b). It can be seen that considering the harmonics up to $\pm 2f_s$ is sufficient to represent the dynamical impacts of grid unbalance, and the fundamental frequency of the Fourier series can be selected as $2f_s$. Therefore, the variable representation considering the ac-dc frequency coupling relationship allows for truncating the HTFs with a minimum order, which is 3 under the unbalanced grids. It is worth noting that this model can be also seen as an extension of the converter model in balanced grids. For balanced conditions, the steady-state trajectories only have dc components, thus the frequency-domain model is represented by LTI transfer functions.

2) HTFS OF DIFFERENT SUBSYSTEMS AND THEIR INTERCONNECTION

Based on the frequency domain model shown in (25), the HTFs of the converter power stage can be derived by $\mathbf{Z}_{\text{ol}}$, $\mathbf{G}_{\text{di}}$, $\mathbf{G}_{\text{vv}}$, $\mathbf{G}_{\text{dv}}$, which denote the input-output relationships from ac voltage to ac current, from ac duty cycle to ac current, from ac voltage to dc voltage, and from ac duty cycle to dc voltage, respectively. Their explicit expressions are provided in Appendix.

The other subsystems, such as PLL, DVC, CC and time delay, can be derived similarly by HTFs considering the same input and output variable representations. The PLL's HTF ($\mathbf{Y}_{\text{PLL}}$) derives the relationship from ac voltage to ac current reference, and the DVC's HTF ($\mathbf{Y}_{\text{DVC}}$) derives the relationship from dc voltage to ac current reference. They are both derived by linearized modeling, since nonlinear Park and inverse Park transformations are involved in the control dynamics. The HTFs of CC and time delay are denoted by $\mathbf{G}_{\text{i}}$ and $\mathbf{G}_{\text{d}}$, respectively, which establish the relationship from the ac current reference to the ac duty cycle. They are linear subsystems, thus the HTFs are derived by frequency shifts of LTI transfer functions, considering the same HTF order as for nonlinear subsystems. The detailed linearized modeling for converter control loops has been introduced in [17], and the modeling principles are the same as for the power stage, thus only the resulted HTFs are provided in Appendix for simplicity.
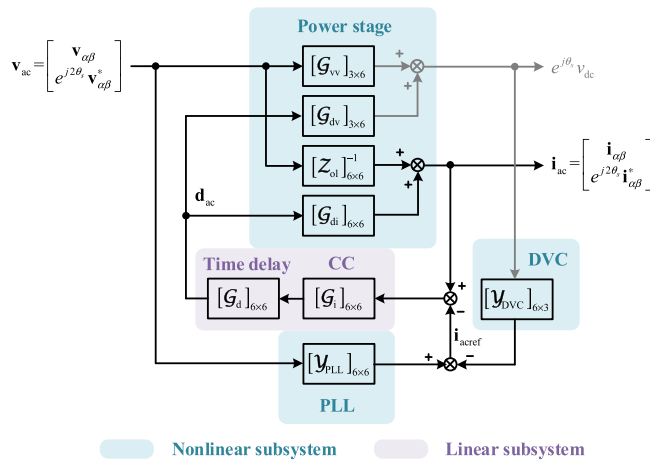
FIGURE 9. Closed-loop frequency-domain model of the converter under unbalanced grid condition.
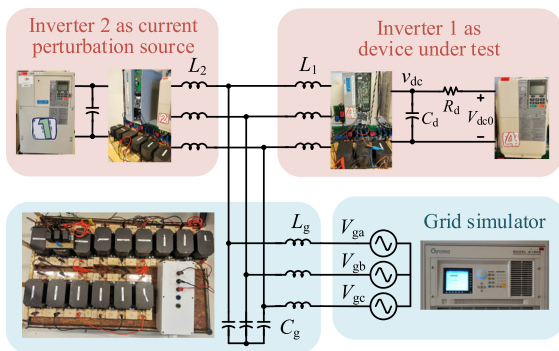

FIGURE 10. Experimental setup for admittance measurement.

TABLE 2. System Parameters for Frequency Scan

Parameter	Value	Parameter	Value
V_{ga}, V_{gb}	110Vrms	V_{gc}	30Vrms
L_g (ESR)	11mH (0.3Ω)	L_1 (ESR)	2mH (0.1Ω)
C_g	21μF	L_2 (ESR)	2mH (0.1Ω))
C_d	0.45μF	R_d	11Ω
V_{dc0}	650V	V_{dc}	620V
f_1	50Hz	f_s (=f_{sw}) / T_s	10kHz / 0.1ms

The ac input admittance of the converter system is calculated and measured for comparison. According to Fig. 9, the analytical model of the converter input admittance can be derived as

$$
\begin{bmatrix}
\mathbf{I}_{\alpha\beta}(s-2j\omega_s) \\
\mathbf{I}_{\alpha\beta}(s) \\
\mathbf{I}_{\alpha\beta}(s+2j\omega_s) \\
e^{j2\varphi^+}\mathbf{I}_{\alpha\beta}^*(s-4j\omega_s) \\
e^{j2\varphi^+}\mathbf{I}_{\alpha\beta}^*(s-2j\omega_s) \\
e^{j2\varphi^+}\mathbf{I}_{\alpha\beta}^*(s)
\end{bmatrix}
= \mathsf{Y}_{ac}
\begin{bmatrix}
\mathbf{V}_{\alpha\beta}(s-2j\omega_s) \\
\mathbf{V}_{\alpha\beta}(s) \\
\mathbf{V}_{\alpha\beta}(s+2j\omega_s) \\
e^{j2\varphi^+}\mathbf{V}_{\alpha\beta}^*(s-4j\omega_s) \\
e^{j2\varphi^+}\mathbf{V}_{\alpha\beta}^*(s-2j\omega_s) \\
e^{j2\varphi^+}\mathbf{V}_{\alpha\beta}^*(s)
\end{bmatrix}
\tag{26}
$$

where $\mathbf{Y}_{ac}$ is truncated as a 6-by-6 HTF expressed by

$$
\mathcal{Y}_{ac} = \left[\mathbf{I} - \mathcal{G}_{di}(\mathbf{I} - \mathcal{G}_d\mathcal{G}_i\mathcal{Y}_{DVC}\mathcal{G}_{dv})^{-1}\mathcal{G}_d\mathcal{G}_i\right]^{-1} \cdot
$$
$$
\left[\mathcal{Z}_{ol}^{-1} - \mathcal{G}_{di}(\mathbf{I} - \mathcal{G}_d\mathcal{G}_i\mathcal{Y}_{DVC}\mathcal{G}_{dv})^{-1}\mathcal{G}_d\mathcal{G}_i \right.
$$
$$
\left. (\mathcal{Y}_{PLL} - \mathcal{Y}_{DVC}\mathcal{G}_{vv})\right]
\tag{27}
$$

where $\mathbf{I}$ is an identity matrix. Since the admittance model is truncated by a 6-by-6 matrix, the frequency scan measurement should inject perturbations 6 times to measure all the elements of (27) [46]. The frequency is scanned within the fundamental frequency interval of the HTF model, i.e., (0, 100) Hz. The frequency responses beyond this interval is unnecessary since they are merely folded from the frequency responses in the fundamental frequency interval [26].

Fig. 11 shows the admittance measurement results of all the elements by simulation first. The asterisks denote the measured results and the solid lines denote the analytical models. It can be seen that almost all the elements of the admittance model can be accurately predicted by frequency scan. There are only small errors in a few elements, which are the elements at the edge of the truncated HTF model. These errors are inevitable due to the HTF model truncation. Fig. 12 further provides the experimental results. For simplicity, only one-column elements in Y_{ac} (e.g., the second column) are plotted on Bode diagrams, where the close agreement also verifies the accuracy of the model.

Then, considering the interconnection of the power stage and different control loops, the closed-loop frequency-domain model of the converter system can be depicted as Fig. 9. This model characterizes the frequency coupling relationships between ac and dc variables and retains the control structure, which enables to derive HTFs from any input to any output.

3) FREQUENCY-SCAN VALIDATION
To validate the frequency-domain modeling, the frequency scan measurements by simulations and experiments on a three-phase converter under unbalanced grid conditions are carried out. The experimental setup is shown in Fig. 10. Inverter 1 is the device under test, which runs with the control scheme in Fig. 4 and the control parameters in Table 1. Inverter 2 is controlled as a current source to inject perturbations by frequency scan. The grid voltage is emulated by a grid simulator (Chroma 61845). Some LC filters are connected between the converters and the grid simulator to emulate the grid impedance. The converter controls are implemented in DS1007. The system parameters are provided in Table 2. The same simulation for frequency scan is established in MATLAB/Simulink.

D. ENGINEERING PERSPECTIVES ON PRACTICAL IMPLEMENTATIONS
Through the case study of the three-phase converter, the benefits of the unified modeling framework in practical implementations from the engineering perspectives can be summarized as follows:
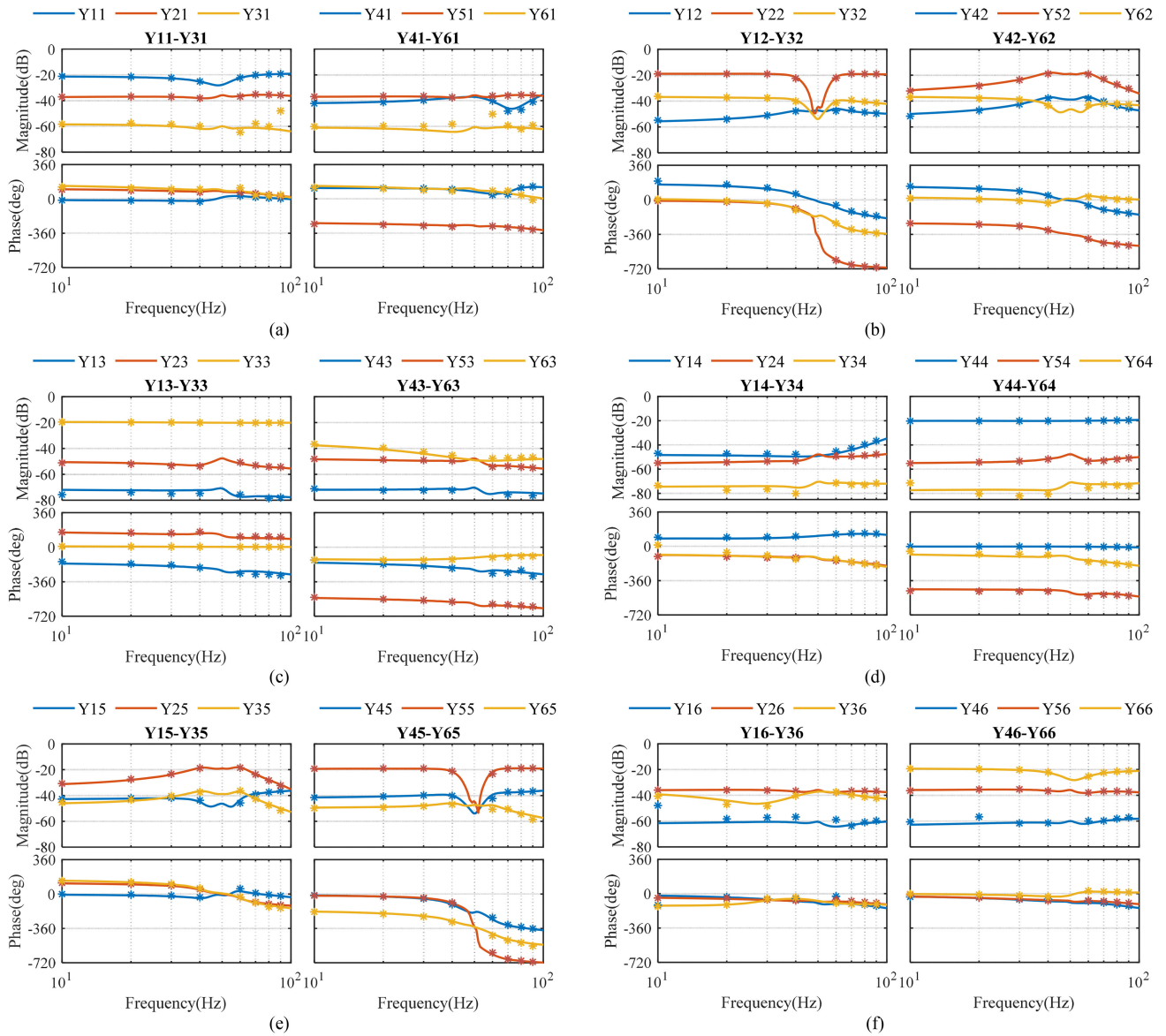
FIGURE 11. Converter ac admittance measurement by simulation. (a)-(f) 1st-6th column elements.
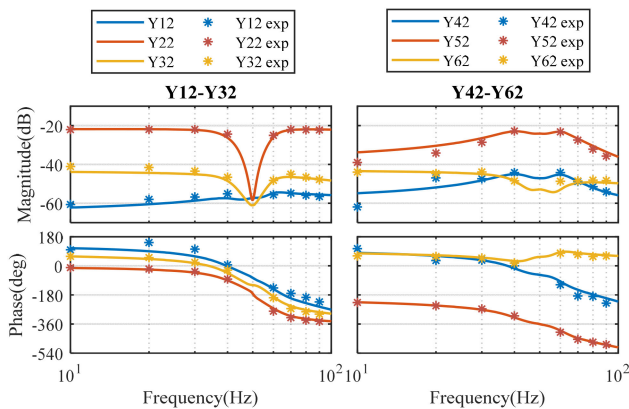

FIGURE 12. Converter ac admittance measurement by experiment.

- *Modular and scalable modeling:* Any system, which can be either a simple control loop or a complex converter system, can be characterized by a unified HTF model, no matter using which modeling methods or following which modeling procedures. Such a model can be easily interconnected to other system and thus facilitates to a modular and scalable modeling, such as Fig. 9. For three-phase converter systems, the three-port variable definitions in [12] are scalable for both balanced systems and unbalanced systems, which can not only characterize the frequency-coupling dynamics caused by converter controls, but also simplify the HTF order when the system is unbalanced, as clarified in Section IV-C-1).

- *Efficient modeling based on system steady states:* thanks to the equivalence and relationships among different

modeling methods, the Toeplitz matrices can also be used to establish the DP and GDQ models based on the DFT analysis of the system steady states, as shown in (17) and (21). Thus, even if the time-domain DP or GDQ model is desired, the modeling efficiency can be improved, since it is not necessary to derive analytically by the GA operators or GDQ transformations.

- *Applicability for black-box systems:* the frequency-domain validation for the converter operating in unbalanced grids also shows that the unified HTF model can characterize the system dynamics accurately even though the system internal parameters are unknown. In actual power systems, the system operating conditions can be complicated and the converter controls can be confidential, the unified HTF model representation can be more practical than other linearized time-domain modeling methods.

V. CONCLUSION

This paper has derived a unified small-signal modeling framework for ac power electronic systems. The framework not only summarizes the existing relationships among different modeling methods, but also reveals some missing ones including

- The linearization and transformation can be exchanged flexibly in the modeling process;
- The initial-phase impact needs to be considered for the GDQ modeling in relation to the HSS or DP modeling.

The unified modeling framework brings some benefits in modeling flexibility and efficiency for ac power electronic systems in more generic grid conditions, which are summarized through a case study on a three-phase converter in unbalanced grids. It has been proved that the converter power stage and the control loops can all be characterized by a unified HTF model. The impact of variable representations on the HTF truncation order has also been discussed. It is revealed that the HTF order can be minimized if the converter ac-dc frequency coupling relationships are considered by exponential functions in the variable representations.

Time domain simulations and frequency-domain experiments have been conducted to validate the theoretical analyses. The frequency-domain validation also proves the advantage of the unified HTF model in modeling black-box dynamics of vendor-specific systems.

APPENDIX

Closed-Loop HTF Models:

1) HTFs of power stage

$$\mathsf{Z}_{\text{ol}} = \mathsf{Z}_{\text{ac}} + \begin{bmatrix} \mathcal{D}_{dq} \\ \mathcal{D}_{dq}^* \end{bmatrix} \frac{\mathsf{Z}_{\text{dc}}(s - j\omega_s)}{2} \begin{bmatrix} \mathcal{D}_{dq}^* & \mathcal{D}_{dq} \end{bmatrix} \quad \text{(A1)}$$

$$\mathsf{G}_{\text{di}} = -\mathsf{Z}_{\text{ol}}^{-1} \left(\begin{bmatrix} \mathcal{V}_{\text{dc}} \\ & \mathcal{V}_{\text{dc}} \end{bmatrix} \right.$$
$$\left. + \begin{bmatrix} \mathcal{D}_{dq} \\ \mathcal{D}_{dq}^* \end{bmatrix} \frac{\mathsf{Z}_{\text{dc}}(s - j\omega_s)}{2} \begin{bmatrix} \mathcal{I}_{dq}^* & \mathcal{I}_{dq} \end{bmatrix} \right) \quad \text{(A2)}$$

$$\mathsf{G}_{\text{vv}} = \left(\mathbf{I} + \frac{\mathsf{Z}_{\text{dc}}(s - j\omega_s)}{2} \begin{bmatrix} \mathcal{D}_{dq}^* & \mathcal{D}_{dq} \end{bmatrix} \mathsf{Z}_{\text{ac}}^{-1} \begin{bmatrix} \mathcal{D}_{dq} \\ \mathcal{D}_{dq}^* \end{bmatrix} \right)^{-1}$$
$$\cdot \frac{\mathsf{Z}_{\text{dc}}(s - j\omega_s)}{2} \begin{bmatrix} \mathcal{D}_{dq}^* & \mathcal{D}_{dq} \end{bmatrix} \mathsf{Z}_{\text{ac}}^{-1} \quad \text{(A3)}$$

$$\mathsf{G}_{\text{dv}} = \left(\mathbf{I} + \frac{\mathsf{Z}_{\text{dc}}(s - j\omega_s)}{2} \begin{bmatrix} \mathcal{D}_{dq}^* & \mathcal{D}_{dq} \end{bmatrix} \mathsf{Z}_{\text{ac}}^{-1} \begin{bmatrix} \mathcal{D}_{dq} \\ \mathcal{D}_{dq}^* \end{bmatrix} \right)^{-1}$$
$$\cdot \frac{\mathsf{Z}_{\text{dc}}(s - j\omega_s)}{2}$$
$$\times \left(\begin{bmatrix} \mathcal{I}_{dq}^* & \mathcal{I}_{dq} \end{bmatrix} - \begin{bmatrix} \mathcal{D}_{dq}^* & \mathcal{D}_{dq} \end{bmatrix} \mathsf{Z}_{\text{ac}}^{-1} \begin{bmatrix} \mathcal{V}_{\text{dc}} \\ & \mathcal{V}_{\text{dc}} \end{bmatrix} \right) \quad \text{(A4)}$$

where $\quad \mathsf{Z}_{\text{ac}} = \begin{bmatrix} \mathsf{Z}_{\text{L}}(s) \\ & \mathsf{Z}_{\text{L}}(s - j2\omega_s) \end{bmatrix}, \quad \mathsf{Z}_{\text{L}}(s) =$
$\begin{bmatrix} (s - j2\omega_s)L \\ & sL \\ & & (s + j2\omega_s)L \end{bmatrix}, \quad \mathsf{Z}_{\text{dc}}(s) =$
$\begin{bmatrix} \frac{1}{(s - j2\omega_s)C} \\ & \frac{1}{sC} \\ & & \frac{1}{(s + j2\omega_s)C} \end{bmatrix}, \quad \mathcal{V}_{\text{dc}}, \mathcal{D}_{dq}, \mathcal{I}_{dq}$ are 3-by-3

HTFs obtained by steady-state trajectories.

2) HTF of PLL

$$\mathsf{Y}_{\text{PLL}} = \frac{1}{2} \begin{bmatrix} \mathcal{I}_{dq\text{ref}} \mathsf{T}_{\Delta\theta} \mathsf{G}_{\text{PLL}}(s - j\omega_s) \mathsf{T}_{\Delta\theta}^* & -\mathcal{I}_{dq\text{ref}} \mathsf{T}_{\Delta\theta} \\ \mathsf{G}_{\text{PLL}}(s - j\omega_s) \mathsf{T}_{\Delta\theta} \\ -\mathcal{I}_{dq\text{ref}}^* \mathsf{T}_{\Delta\theta}^* \mathsf{G}_{\text{PLL}}(s - j\omega_s) \mathsf{T}_{\Delta\theta}^* & \mathcal{I}_{dq\text{ref}}^* \\ \mathsf{T}_{\Delta\theta}^* \mathsf{G}_{\text{PLL}}(s - j\omega_s) \mathsf{T}_{\Delta\theta} \end{bmatrix} \quad \text{(A5)}$$

where $\quad \mathsf{G}_{\text{PLL}}(s) = (I + G_{\text{Notch-PI-I}}(s)V_d^c)^{-1} G_{\text{Notch-PI-I}}(s)$,
$\mathsf{G}_{\text{Notch-PI-I}} = diag \left\{ \begin{matrix} G_{\text{Notch-PI-I}}(s - j2\omega_s), G_{\text{Notch-PI-I}}(s) \\ , G_{\text{Notch-PI-I}}(s + j2\omega_s) \end{matrix} \right\}$
and $G_{\text{Notch-PI-I}}(s)$ is the transfer function of the PLL including the notch filter, the PI controller and the integrator.

$\mathsf{T}_{\Delta\theta}$ is the HTF of $e^{j\Delta\theta}$, where $\Delta\theta$ is the steady-state phase difference between the PLL control dq frame and the positive-sequence system dq frame [17]. V_d^c is the HTF of $V_d^c(t)$, which is the steady-state d-axis voltage in PLL control dq frame. $\mathcal{I}_{dq\text{ref}}$ is the HTF of the steady-state $I_{dq\text{ref}}(t)$.

3) HTF of DVC

$$\mathsf{Y}_{\text{DVC}} = \begin{bmatrix} \mathsf{T}_{\Delta\theta} \mathsf{G}_{\text{DVC}}(s - j\omega_s) \\ \mathsf{T}_{\Delta\theta} \mathsf{G}_{\text{DVC}}(s - j\omega_s) \end{bmatrix} \quad \text{(A6)}$$

where $\quad \mathsf{G}_{\text{DVC}}(s) = diag\{G_{\text{dvc}}(s - j2\omega_s), \quad G_{\text{dvc}}(s),$
$G_{\text{dvc}}(s + j2\omega_s)\}$ and $G_{\text{dvc}}(s)$ is the transfer function of the DVC PI controller.

4) HTFs of CC and time delay

$$\mathsf{G}_{\text{i}} = \frac{1}{V_{\text{dc}}} \begin{bmatrix} \mathsf{G}_{\text{CC}}(s) \\ & \mathsf{G}_{\text{CC}}(s - 2j\omega_s) \end{bmatrix} \quad \text{(A7)}$$

where $\quad \mathsf{G}_{\text{CC}}(s) = diag\{G_i(s - j2\omega_s), G_i(s), G_i(s + j2\omega_s)\}$ and $G_i(s)$ is the transfer function of the CC PR controller.

$$\mathsf{G}_{\text{d}} = \begin{bmatrix} \mathsf{G}_{\text{delay}}(s) \\ & \mathsf{G}_{\text{delay}}(s - 2j\omega_s) \end{bmatrix} \quad \text{(A8)}$$

where $\mathsf{G}_{\text{delay}}(s) = diag\{G_d(s - j2\omega_s), G_d(s), G_d(s + j2\omega_s)\}$ and $G_d(s)$ is the transfer function of the time delay, which is modeled by e^{-sTd} [5].

REFERENCES

[1] X. Wang and F. Blaabjerg, "Harmonic stability in power electronic based power systems: Concept, modeling, and analysis," *IEEE Trans. Smart Grid*, vol. 10, no. 3, pp. 2858−2870, May 2019.

[2] G. W. Wester and R. D. Middlebrook, "Low-frequency characterization of switched dc-dc converters," *IEEE Trans. Aero. Electron. Syst.*, vol. AES-9, no. 3, pp. 376–385, May 1973.

[3] R. D. Middlebrook and S. Cuk, "A general unified approach to modeling switching converter power stages," in *Proc. IEEE Power Electron. Spec. Conf.*, 1976, pp. 18–34.

[4] S. Hiti, D. Boroyevich, and C. Cuadros, "Small-signal modeling and control of three-phase PWM converters," in *Proc. IEEE Ind. Appl. Soc. Annu. Meeting*, Denver, CO, USA, Oct. 1994, pp. 1143–1150.

[5] L. Harnefors, M. Bongiorno, and S. Lundberg, "Input-admittance calculation and shaping for controlled voltage-source converters," *IEEE Trans. Ind. Electron.*, vol. 54, no. 6, pp. 3323–3334, Nov. 2007.

[6] B. Wen, D. Boroyevich, R. Burgos, P. Mattavelli, and Z. Shen, "Analysis of D-Q small-signal impedance of grid-tied inverters," *IEEE Trans. Power Electron.*, vol. 31, no. 1, pp. 675–687, Jan. 2016.

[7] L. Harnefors, "Modeling of three-phase dynamic systems using complex transfer functions and transfer matrices," *IEEE Trans. Ind. Electron.*, vol. 54, no. 4, pp. 2239–2248, Aug. 2007.

[8] Y. Gu, Y. Li, Y. Zhu, and T. Green, "Impedance-based whole-system modeling for a composite grid via embedding of frame dynamics," *IEEE Trans. Power Syst.*, vol. 36, no. 1, pp. 336–345, Jan. 2021.

[9] A. Rygg, M. Molinas, C. Zhang, and X. Cai, "A modified sequence-domain definition and its equivalence to dq-domain impedance definition for the stability analysis of AC power electronic systems," *IEEE J. Emerg. Sel. Topics Power Electron.*, vol. 4, no. 4, pp. 1383–1396, Dec. 2016.

[10] C. T. Rim, "Unified general phasor transformation for AC converters," *IEEE Trans. Power Electron.*, vol. 26, no. 9, pp. 2465–2475, Sep. 2011.

[11] X. Wang, L. Harnefors, and F. Blaabjerg, "Unified impedance model of grid-connected voltage-source converters," *IEEE Trans. Power Electron.*, vol. 33, no. 2, pp. 1775–1787, Feb. 2018.

[12] Y. Liao and X. Wang, "Stationary-frame complex-valued frequency-domain modeling of three-phase power converters," *IEEE J. Emerg. Sel. Topics Power Electron.*, vol. 8, no. 2, pp. 1922–1933, Jun. 2020.

[13] E. Mollerstedt and B. Bernhardsson, "Out of control because of harmonics-an analysis of the harmonic response of an inverter locomotive," *IEEE Control Syst. Mag.*, vol. 20, no. 4, pp. 70–81, Aug. 2000.

[14] T. Noda, A. Semlyen, and R. Iravani, "Harmonic domain dynamic transfer function of a nonlinear time-periodic network," *IEEE Trans. Power Del.*, vol. 18, no. 4, pp. 1433–1441, Oct. 2003.

[15] J. Lyu, X. Zhang, X. Cai, and M. Molinas, "Harmonic state-space based small-signal impedance modeling of a modular multilevel converter with consideration of internal harmonic dynamics," *IEEE Trans. Power Electron.*, vol. 34, no. 3, pp. 2134–2148, Mar. 2019.

[16] H. Wu and X. Wang, "Dynamic impact of zero-sequence circulating current on modular multilevel converters: Complex-valued ac impedance modeling and analysis," *IEEE J. Emerg. Sel. Topics Power Electron.*, vol. 8, no. 2, pp. 1947–1963, Jun. 2020.

[17] Y. Liao, X. Wang, X. Yue, and L. Harnefors, "Complex-valued multifrequency admittance model of three-phase VSCs in unbalanced grids," *IEEE J. Emerg. Sel. Topics Power Electron.*, vol. 8, no. 2, pp. 1934–1946, Jun. 2020.

[18] H. Yang, H. Just, M. Eggers, and S. Dieckerhoff, "Linear time-periodic theory based modeling and stability analysis of voltage source converters," *IEEE J. Emerg. Sel. Topics Power Electron.*, vol. 9, no. 3, pp. 3517–3529, Jun. 2021.

[19] P. C. Stefanov and A. M. Stankovic, "Modeling of UPFC operation under unbalanced conditions with dynamic phasors," *IEEE Trans. Power Syst.*, vol. 17, no. 2, pp. 395–403, May 2002.

[20] J. J. Rico, M. Madrigal, and E. Acha, "Dynamic harmonic evolution using the extended harmonic domain," *IEEE Trans. Power Del.*, vol. 18, no. 2, pp. 587–594, Apr. 2003.

[21] O. C. Sakinci and J. Beerten, "Generalized dynamic phasor modeling of the MMC for small-signal stability analysis," *IEEE Trans. Power Del.*, vol. 34, no. 3, pp. 991–1000, Jun. 2019.

[22] P. J. Hart, J. Goldman, R. H. Lasseter, and T. M. Jahns, "Impact of harmonics and unbalance on the dynamics of grid-forming, frequency-droop-controlled inverters," *IEEE J. Emerg. Sel. Topics Power Electron.*, vol. 8, no. 2, pp. 976–990, Jun. 2020.

[23] P. Rioual, H. Pouliquen, and J. -P. Louis, "Regulation of a PWM rectifier in the unbalanced network state using a generalized model," *IEEE Trans. Power Electron.*, vol. 11, no. 3, pp. 495–502, May 1996.

[24] A. Jamshidifar and D. Jovcic, "Small-signal dynamic DQ model of modular multilevel converter for system studies," *IEEE Trans. Power Del.*, vol. 31, no. 1, pp. 191–199, Feb. 2016.

[25] T. Li, A. M. Gole, and C. Zhao, "Harmonic instability in MMC-HVDC converters resulting from internal dynamics," *IEEE Trans. Power Del.*, vol. 31, no. 4, pp. 1738–1747, Aug. 2016.

[26] N. M. Wereley, "Analysis and control of linear periodically time varying systems," Ph.D. dissertation, Dept. Aeronautics Astronautics, MIT, 1991.

[27] A. Packard, K. Poolla, and R. Horowitz, "Dynamic systems and feedback class notes," Dept. Mech. Eng., Univ. California, Berkeley, CA, USA, 2002. [Online]. Available: https://www.cds.caltech.edu/~murray/courses/cds101/fa02/caltech/pph.html

[28] J. Sun, "Small-signal methods for AC distributed power systems–A review," *IEEE Trans. Power Electron.*, vol. 24, no. 11, pp. 2545–2554, Nov. 2009.

[29] H. Sandberg, E. Mollerstedt, and B. Bernhardsson, "Frequency-domain analysis of linear time-periodic systems," *IEEE Trans. Auto. Cont.*, vol. 50, no. 12, pp. 1971–1983, Dec. 2005.

[30] Y. Li, Y. Gu, and T. C. Green, "Interpreting frame transformations in AC systems as diagonalization of harmonic transfer functions," *IEEE Trans. Circle Syst. I: Reg. Papers*, vol. 67, no. 7, pp. 2481–2491, Jul. 2020.

[31] S. R. Sanders, J. M. Noworolski, X. Z. Liu, and G. C. Verghese, "Generalized averaging method for power conversion circuits," *IEEE Trans. Power Electron.*, vol. 6, no. 2, pp. 251–259, Apr. 1991.

[32] D. Maksimovic, A. M. Stankovic, V. J. Thottuvelil, and G. C. Verghese, "Modeling and simulation of power electronic converters," in *Proc. IEEE*, vol. 89, no. 6, pp. 898–912, Jun. 2001.

[33] X. Yue, X. Wang, and F. Blaabjerg, "Review of small-signal modeling methods including frequency-coupling dynamics of power converters," *IEEE Trans. Power Electron.*, vol. 34, no. 4, pp. 3313–3328, Apr. 2019.

[34] S. D. Sudhoff, "Multiple reference frame analysis of an unsymmetrical induction machine," *IEEE Trans. Energy Conv.*, vol. 8, no. 3, pp. 425–432, Sep. 1993.

[35] J. Groves, "Small-signal analysis using harmonic balance methods," in *Proc. IEEE Power Electron. Spec. Annu. Conf.*, Cambridge, MA, USA, 1991, pp. 74–79.

[36] J. E. Ormrod, "Analysis and control of linear periodically time varying systems," M.E. thesis, Elect. Comput. Eng., University of Canterbury, 2013.

[37] J. Kwon, X. Wang, F. Blaabjerg, C. L. Bak, A. R. Wood, and N. R. Watson, "Linearized modeling methods of AC–DC converters for an accurate frequency response," *IEEE J. Emerg. Sel. Topics Power Electron.*, vol. 5, no. 4, pp. 1526–1541, Dec. 2017.

[38] P. D. Rua, O. C. Sakinci, and J. Beerten, "Comparative study of dynamic phasor and harmonic state-space modeling for small-signal stability analysis," *Elect. Power Syst. Res.*, vol. 189, Dec. 2020, Art. no. 106626.

[39] N. Blin, P. Riedinger, J. Daafouz, L. Grimaud, and P. Feyel, "A comparison of harmonic modeling methods with application to the interconnection and the control of switched systems," *Eur. J. Control*, vol. 58, pp. 245–257, Mar. 2021.

[40] O. C. Sakinci and J. Beerten, "Equivalent multiple dq-frame model of the MMC using dynamic phasor theory in the $\alpha\beta z$-frame," *IEEE Trans. Power Del.*, vol. 35, no. 6, pp. 2916–2927, Dec. 2020.

[41] Z. Xu, B. Li, S. Zhang, L. Han, J. Hu, and D. Xu, "Study on equivalence of MMC modeling under multi-dq frames and harmonic state space," in *Proc. 8th Renew. Power Gen. Conf.*, Shanghai, China, 2019, pp. 1–6.

[42] A. Rygg, "Impedance-based methods for small-signal analysis of systems dominated by power electronics," Ph.D. dissertation, Dept. Engineering Cybern., Norwegian Univ. Sci. Technol., Trondheim, Norway, 2018.

[43] M. H. Hirsch, S. Smale, and R. L. Devaney, *Differential Equations, Dynamical Systems & An Introduction to Chaos*, 3rd ed., Amsterdam, Netherlands: Elsevier, 2013.

[44] M. Reed and B. Simon, *Methods of Modern Mathematical Physics: Functional Analysis*. Waltham, MA, USA: Academic Press, 1972.

[45] S. Yamamura, *Spiral Vector Theory of AC Circuits and Machines*. New York, NY, USA: Oxford Univ. Press, 1992.

[46] V. Salis, A. Costabeber, S. M. Cox, F. Tardelli, and P. Zanchetta, "Experimental validation of harmonic impedance measurement and LTP nyquist criterion for stability analysis in power converter networks," *IEEE Trans. Power Electron.*, vol. 34, no. 8, pp. 7972–7982, Aug. 2019.

YICHENG LIAO (Member, IEEE) received the B.S. and M.S. degrees in electrical engineering from Southwest Jiaotong University, Chengdu, China, in 2015 and 2018, respectively, and the Ph.D. degree in energy technology from Aalborg University, Aalborg, Denmark, in 2021. In July 2017, she was a Visiting Student with Ecole Polytechnique and French National Institute for Research in Digital Science and Technology, Paris, France. From September 2018 to July 2021, she was with the AAU Energy, Aalborg University, as a Research Assistant and later on a Postdoc. Since August 2021, she has been a Postdoc with the School of Electrical Engineering and Computer Science, KTH Royal Institute of Technology, Stockholm, Sweden. Her research focuses on the modeling, stability analysis, and control of power electronics-based power systems. She was selected as the 2020 Outstanding Reviewer of the IEEE TRANSACTIONS ON POWER ELECTRONICS and the 2020 Star Reviewer of the IEEE JOURNAL OF EMERGING AND SELECTED TOPICS IN POWER ELECTRONICS. She was the recipient of the 2020 Top Download Paper Award from the IEEE OPEN JOURNAL OF THE INDUSTRIAL ELECTRONICS SOCIETY and the 2021 Ph.D. Thesis Talk Award from the IEEE Power Electronics Society.

XIONGFEI WANG (Senior Member, IEEE) received the B.S. degree in electrical engineering from Yanshan University, Qinhuangdao, China, in 2006, the M.S. degree in electrical engineering from Harbin Institute of Technology, Harbin, China, in 2008, and the Ph.D. degree in energy technology from Aalborg University, Aalborg, Denmark, in 2013. Since 2009, he has been with the Department of Energy Technology, Aalborg University, where he became an Assistant Professor in 2014, an Associate Professor in 2016, a Professor and Leader of Electronic Power Grid Research Group in 2018. Since 2020, he has also been a Visiting Professor with the KTH Royal Institute of Technology, Stockholm, Sweden. His current research interests include modeling and control of power electronic converters and systems, stability and power quality of power-electronics-dominated power systems, and high-power converters. He is a Member-at-Large of Administrative Committee for the IEEE Power Electronics Society (PELS) during 2020–2022, the Co-Editor-in-Chief of the IEEE TRANSACTIONS ON POWER ELECTRONICS LETTERS, and as an Associate Editor for the IEEE JOURNAL OF EMERGING AND SELECTED TOPICS IN POWER ELECTRONICS. In 2016, he was selected into Aalborg University Strategic Talent Management Program. He was the recipient of six Prize Paper Awards in the IEEE transactions and conferences, the 2018 Richard M. Bass Outstanding Young Power Electronics Engineer Award, the 2019 IEEE PELS Sustainable Energy Systems Technical Achievement Award, the 2020 IEEE Power & Energy Society Prize Paper Award, the 2020 JESTPE Star Associate Editor Award, and the Highly Cited Researcher in the Web of Science during 2019–2020.